# Adjoint of a Parameterized Moisture Convection Model

Robert G. Fovell
Department of Atmospheric Sciences
University of California, Los Angeles
With 15 Figures

April 23, 2003

## Summary

Adjoint models have found use as "dynamical tracers", helping to track a feature or phenomenon back to its origin. Their application to the study of atmospheric convection, however, is challenged by the complexity and nonlinearity of diabatic processes. Herein, the adjoint of a significantly simpler parameterized moisture (PM) model is described and tested. The PM model eliminates explicit moisture by making latent heating conditionally proportional to updraft velocity and providing a lower tropospheric heat sink mimicking rainwater evaporation.

The PM adjoint, of course, is useful only if the parameterization can produce realistic results. Earlier work suggested that the PM framework possessed a fundamental flaw that made its storms have an excessive impact on their upstream environments. In fact, the adjoint was used to identify the origin of the discrepancies between PM and traditional cloud model storms, thereby leading to the parameterization improvements and dynamical insights recently discussed in Fovell (2002). The present paper is a companion to that study, describing how the adjoint model was constructed, tested and utilized. In addition, an even more realistic adjoint framework is described.

## 1 Introduction

One of the modeler's most difficult tasks is to successfully identify the source of a particular phenomenon or result. Hypothesis testing often means altering model prognostic fields, parameter settings, numerical techniques and/or boundary conditions and rerunning the model – sometimes many, many times. Diagnosing which parameters, fields, locales and/or times are the most likely candidates for alteration can be quite a challenge. Even if our hypotheses are correct, the perturbations we apply in the test runs may have unanticipated, wide-ranging effects that tend to obscure the very confirmation we seek. It would be more straightforward if we could just run the models backward to trace a feature to its origin, but few nonlinear models are amenable to this procedure.

"Adjoint models" are increasingly being used in such situations (e.g., Errico 1997). Unlike a forward model which forecasts temperatures, winds, humidities and the like forward in time from a presumed known state, the adjoint propagates *sensitivities* with respect to those fields, as well

as model parameters, backwards in time from a specified "final" sensitivity condition designed to test one's hypothesis. The adjoint is the transpose of the "tangent linear model", itself a forward integrated model linearized about the temporally and spatially varying state provided by the control simulation under scrutiny. Adjoint models are being used operationally for data assimilation (e.g., Talagrand and Courtier, 1987; Ghil et al., 1997), forecast error source tracking (e.g., Rabier et al., 1996; Reed et al., 2001) and optimal observational siting tasks (e.g., Lorenz and Emanuel, 1998; Langland et al., 1999), among other uses. Errico and Vukicevic (1992; "EV") presented not only an accessible description of adjoint model construction but also a very nice demonstration of how adjoint-derived sensitivity fields can be interpreted. Many sensitivity studies focus on synoptic or meso-alpha scale phenomena though applications to smaller scale flows have been appearing as well (e.g., Park and Droegemeier, 1999, 2000).

One major challenge facing adjoint usage for convective scale problems is the significant complexity and nonlinearity of the diabatic processes, in particular those involving water substance. Herein we describe and employ the adjoint of a *parameterized moisture* (PM) convection model, similar to that used to examine dynamics of squall-line storms by Garner and Thorpe (1992) and Fovell and Tan (2000; "FT2000"). The moisture parameterization obviates the explicit treatment of water substance and latent heating and cooling. In particular, condensation heating is made conditionally proportional to vertical velocity, and evaporation cooling is handled by a simple sponge-type term. Traditional explicit moisture cloud models usually track at least three forms of water and possess microphysical interaction terms with "on/off" switches which are tricky to handle in adjoint models (Xu, 1996; Zou, 1997). The PM model's dramatically simplified moisture treatment greatly reduces the complexity of the adjoint, facilitating its construction and perhaps permitting relatively more accurate results as well.

Naturally, the PM adjoint is of little or no value unless the PM model framework itself performs adequately relative to traditional models. FT2000's evaluation of the PM model for squall-line simulations demonstrated that it could capture the temporal unsteadiness of commonly occurring "multicellular" convection despite its simplifications. However, its model storms were found to vary from their explicit moisture counterparts with regard to the magnitude of their "upstream" influences. Convective storms modify their surroundings, including the upstream environments into which they are propagating, with important feedbacks onto the storm itself. The PM model storm

was judged to induce a lower tropospheric inflow that was far too strong relative to typical cloud model results.

FT2000 hypothesized the PM approach possessed a fundamental flaw which permitted excessive warming to accumulate on the storm's downstream (trailing) environment. Attempts to "fix" the PM model by restraining those thermal perturbations, however, did not really work. Recently, Fovell (2002) showed that rather than the presence of extensive warming on the storm's downstream side it was the *absence* of quite small, localized and yet persistent cooling on the *upstream* side that explained the differences between the PM and explicit moisture model storms. We didn't wish to construct the PM model adjoint until the framework's results were more realistic. As it happened, the *adjoint was instrumental in identifying the source of the discrepancies, by suggesting where, when and which fields to examine.*

In this paper, we describe how the PM model adjoint was constructed, tested and vetted, and the manner in which it contributed to the Fovell (2002) analysis. The present work should be considered a companion paper to the Fovell (2002) study.

# 2 Model

## 2.1 Background and terminology

In this section, an overview of adjoint sensitivity analysis is offered, motivating the specific methodology employed in this paper. More comprehensive surveys of adjoint techniques may be found in Cacuci and Hall (1984), Talagrand and Courtier (1987; "TC"), and EV, among other papers.

The modeling system has three components: the nonlinear and tangent linear models, both integrated forward in time, and the adjoint model, operated in reverse. The full nonlinear model may be employed to make two distinct simulations, herein termed the "control" and "alternative" runs, which may have have started with different initial conditions (ICs) and/or parameter settings. The tangent linear model (TLM) is a modified version of the fully nonlinear model that can be thought of as attempting to prognose and track the discrepancies between these two nonlinear model runs. The TLM is obtained by taking the full model's code and linearizing it via truncated Taylor series

about a temporally and spatially evolving state provided by the control simulation.

Thus, an approximation to the alternative run is obtained by combining the control and TLM solutions, its accuracy being dependent upon the importance of the terms missing from the TLM. In our work, the TLM represents the intermediate step in adjoint model construction, mainly used to verify that the adjoint is coded and operating properly. Adjoint simulations commence with the specification of a "forecast aspect" $J$, literally representing some scalar aspect of the nonlinear forecast marked for closer examination (e.g., EV). As an example, we will be basing $J$ on the horizontal velocity within designated regions and attempt to trace the dynamical origins of those velocities.

Symbolically, $\tilde{w}^n_{i,k}$, $w''^n_{i,k}$ and $\hat{w}^n_{i,k}$ will represent versions of the variable $w^n_{i,k}$ from the control, TLM and adjoint solutions, respectively. In this case, the variable identified is the vertical velocity at time $n$ and spatial location $i, k$. The adjoint variable $\hat{w}^n_{i,k}$ is a shorthand for $\frac{\partial \tilde{J}}{\partial \tilde{w}^n_{i,k}}$, and has the units of $J$ divided by those of $w$. It represents the estimated sensitivity of $J$ with respect to the control run's value of $w$ at the designated time and location. In this paper, we consider only forecast aspects defined at a single instant of time, though much more complex formulations are possible (e.g., EV), and do not pursue sensitivities with respect to model parameters.

The adjoint model is obtained by effectively transposing the TLM. The matrix algebra involved is particularly straightforward when a two time level scheme is adopted and parameter variations are neglected (e.g., EV). In this situation, the fully discretized TLM composed of $F$ fields and $G$ gridpoints may be written as

$$\mathbf{x}''^{n+1} = \tilde{\mathbf{A}}_n \mathbf{x}''^n, \tag{1}$$

where $\mathbf{x}''$ is the length $L = F \cdot G$ vector of TLM deviations. The $L \times L$ matrix $\tilde{\mathbf{A}}_n$ is a time-dependent function solely of the control run. Because the model is deterministic, the TLM solution at time $N$ may be written as a unique function of the model state at any earlier time $M$, i.e.,

$$\mathbf{x}''^N = \tilde{\mathbf{P}}_{M,N} \mathbf{x}''^M, \tag{2}$$

where $\tilde{\mathbf{P}}_{M,N} = \tilde{\mathbf{A}}_{N-1} \tilde{\mathbf{A}}_{N-2} \cdots \tilde{\mathbf{A}}_{M+1} \tilde{\mathbf{A}}_M$ and is termed the transition matrix.

Motivated by (1), the discretized adjoint model is formulated as

$$\hat{\mathbf{x}}^n = \tilde{\mathbf{A}}_n^T \hat{\mathbf{x}}^{n+1}, \tag{3}$$

in which $\hat{\mathbf{x}}$ is the length $L$ vector of adjoint sensitivities. The adjoint model integrates backwards, utilizing control run information that was archived during the forward model run. For specified starting condition valid at time $N$, the adjoint sensitivities at the earlier time $M$ are

$$\hat{\mathbf{x}}^M = \tilde{\mathbf{P}}_{M,N}^T \hat{\mathbf{x}}^N. \tag{4}$$

Note the matrices $\tilde{\mathbf{A}}$ and $\tilde{\mathbf{P}}_{M,N}$ have been transposed, not inverted, and the TLM is not directly involved.

We are at least qualitatively concerned with $dJ$, representing the potential change to $\tilde{J}$ owing to alterations to the control run state, as this reveals how the adjoint's predicted sensitivities are interpreted and how the adjoint model is vetted. Conceivably, any variable at any spatial location might effect a change in $\tilde{J}$, so long as there exists nonzero sensitivity to the alteration. The first-order Taylor series approximation to $dJ$ at time $N$ is

$$\Delta J_N = \sum_{l=1}^{L} x_l''^N \frac{\partial \tilde{J}}{\partial \tilde{x}_l^N} = \sum_{l=1}^{L} x_l''^N \hat{x}_l^N \equiv \left\langle \hat{\mathbf{x}}^N, \mathbf{x}''^N \right\rangle. \tag{5}$$

In other words, taking the variable and location represented by $x_l^N$ and applying a permutation ($x_l''^N$) to it will contribute towards altering $J$ depending upon the degree of sensitivity there ($\hat{x}_l^N$).

This is unhelpful, at least at time $N$, since the sensitivities ($\hat{x}_l^N$) represent the adjoint's supplied starting condition and even $\Delta J_N$ may be prescribed by the degree of alteration to the forecast aspect desired. The goal is to reveal which alterations at *earlier times* might effect that *same* final alteration. The requisite sensitivities are obtained through backward integration of the adjoint model and are then related to the desired $\Delta J_N$ via the "adjoint property"

$$\langle \mathbf{a}, \mathbf{L}\mathbf{b} \rangle = \left\langle \mathbf{L}^T \mathbf{a}, \mathbf{b} \right\rangle, \tag{6}$$

where $\mathbf{L}$ is an $L \times L$ matrix and $\mathbf{a}$ and $\mathbf{b}$ are $L$ length vectors. The relationship spanning times $N$ back to $M$ starts with (5) and makes use of (2), (4) and (6):

$$\Delta J_N \quad = \quad \left\langle \hat{\mathbf{x}}^N, \mathbf{x}''^N \right\rangle$$

$$
\begin{aligned}
&= \left\langle \hat{\mathbf{x}}^N, \tilde{\mathbf{P}}_{M,N} \mathbf{x}''^M \right\rangle \\
&= \left\langle \tilde{\mathbf{P}}^T_{M,N} \hat{\mathbf{x}}^N, \mathbf{x}''^M \right\rangle \\
&= \left\langle \hat{\mathbf{x}}^M, \mathbf{x}''^M \right\rangle \equiv \Delta J_M. \qquad (7)
\end{aligned}
$$

Two points have been demonstrated, at least for two time-level models. First, that $\Delta J$ is temporally invariant. This forms the basis of the "gradient test" (e.g., TC; Rosmond 1997), a powerful check on the fidelity of the TLM and adjoint model codes. Second, that (5) holds for any time $n$ and thus alterations should be (quantitatively or conceptually) applied to those fields and gridpoints where nonzero sensitivity exists at that time. To effect a positive change in $J$, a positive (negative) alteration should be applied where positive (negative) sensitivity is predicted.

## 2.2 The moisture parameterization

In this paper, perturbations from any run's horizontally homogeneous, temporally invariant base state are denoted with single primes. As described in FT2000, the PM framework (see Fig. 1) is specifically tailored to the classical squall line's leading-line and trailing stratiform organization and mimicks moisture's first order effects by parameterizing terms representing condensation warming ($Q^+$) and evaporation cooling ($Q^-$) in the perturbation potential temperature ($\theta'$) equation, *viz.*

$$\frac{d\theta'}{dt} = Q^+ + Q^-. \qquad (8)$$

The cooling takes place in a shallow zone in which air is continually relaxed towards a selected potential temperature perturbation, $\theta'_c$, with time scale $\tau_c$. The zone's upstream edge is kept a small distance $\delta$ behind the storm's surface gust front position; this is examined every time step and shifted if necessary. $Q^+$ is handled as

$$Q^+ = \gamma^* \max(w, 0), \qquad (9)$$

where $w$ is vertical velocity and $\gamma^*$ is the specified parcel potential temperature lapse rate, a function of height alone. The model subdomain in which $\gamma^* > 0$, termed the "unstable region", extends to the downstream lateral boundary but is truncated a small distance $\epsilon$ ahead of the gust front. As in FT2000, both $\delta$ and $\epsilon$ are taken to be 5 km.

## 2.3 Basic model design

FT2000's PM model implementation was changed in a variety of ways to simplify adjoint construction. The present model is "quasi-compressible" (Chorin, 1967), discounting the sound speed to 100 m $s^{-1}$ since larger values produced very similar results at greater expense. The upper and lower boundaries are rigid, free-slip plates; the horizontal domain is periodic. The latter forces the use of relatively wider domains though advantageously PM storms tend to develop and mature fairly quickly.

The two-dimensional (2D) model domain is 550 km wide and 21.2 km deep with horizontal and vertical grid spacings of $\Delta x = 1$ km and $\Delta z = 250$ m, respectively. Its staggered "C" grid arrangement (Arakawa and Lamb, 1977) places scalar $\theta'_k$ a distance of $\frac{1}{2}\Delta z$ above and below vertical velocity points $w_k$ and $w_{k+1}$. The time step $\Delta t$ is 0.5 s. Note that "time splitting", the approach that integrates acoustically active and inactive terms with different time steps (e.g., Klemp and Wilhelmson, 1978), was not adopted. We have chosen straightforward over efficient design at this time.

The modeling system can use either the leapfrog or the Euler-backward schemes, both employing second order centered differencing for spatial derivatives. The leapfrog is more efficient but its three time level structure complicates implementation and fidelity assessment of the adjoint model, as well as interpretation of that model's intermediate results (see Appendix). These are the strengths of the two-time level Euler-backward version, though that scheme requires roughly twice the number of computations and tends to damp high frequency signals (Haltiner and Williams, 1980). The latter is not a concern; because the model is compressible and not time split, the modes of interest are actually quite slowly varying. The two versions yield virtually indistinguishable results, for both forward and reverse integrations (the latter being apparent after adjacent time steps are fused in the leapfrog model).

## 2.4 Implementing the parameterization in the TLM

The function $\gamma_*$ is defined at the $w$ locations at the top and bottom of each grid box, being nonzero only within the spatially truncated unstable region. When a two time level scheme is employed, (9) is implemented at time $n$ and scalar spatial location $i, k$ in the nonlinear forward model as

$$Q^+_{i,k} = \frac{\Delta t}{2}\left[\max(w^n_{i,k+1}, 0)\gamma^*_{k+1} + \max(w^n_{i,k}, 0)\gamma^*_k\right]. \tag{10}$$

That is, the parameterized heating is calculated at the adjacent $w$ locations and then averaged to the grid box center where $\theta'$ resides. This means the PM model's discretized latent heating term (10) is a simple function of two vertical velocities

$$Q^+_{i,k} = F\left(w^n_{i,k+1}, w^n_{i,k}\right)$$

making its TLM implementation straightforward. The TLM term, evaluated with respect to the control run, is

$$Q''^+_{i,k} = w''^n_{i,k+1}\left.\frac{\partial F}{\partial w^n_{i,k+1}}\right|_C + w''^n_{i,k}\left.\frac{\partial F}{\partial w^n_{i,k}}\right|_C \tag{11}$$

$$= \frac{\Delta t}{2}\left[\tilde\beta^n_{i,k+1} w''^n_{i,k+1}\gamma^*_{k+1} + \tilde\beta^n_{i,k} w''^n_{i,k}\gamma^*_k\right], \tag{12}$$

presuming that grid location $i, k$ resides in the unstable region. The subscript $C$ in the first expression means the term is evaluated for the control run. In the second, $\tilde\beta$ indicates whether ascent is present in the control run at the given point and time:

$$\tilde\beta^n_{i,k} = \begin{cases} 1 & \tilde w^n_{i,k} > 0; \\ 0 & \text{otherwise.} \end{cases}$$

Parameterized evaporation cooling in the control run is handled as

$$Q^-_{i,k} = -\left(\theta'^n_{i,k} - \theta'_c\right)\tau_c^{-1}, \tag{13}$$

presuming point $i$, $k$ falls within the spatially confined cooling zone. The TLM version of (13) is simply

$$Q''^-_{i,k} = -\theta''^n_{i,k}\tau_c^{-1}, \tag{14}$$

at that point[1]. The position of the cooling zone may shift with time if the control run's specified domain translation speed fails to keep the gust front stationary. Our system forces such shifts to occur at the same time in the TLM and adjoint simulations.

[1] If the leapfrog scheme is employed, the $\theta'$ and $\theta''$ values used must represent the past time step, $n-1$, for stability.

### 2.5 Adjoint implementations of the parameterization

Now we turn to the adjoint formulations. Starting with (12) and (14) the adjoint was constructed by hand transposition following EV's recipe. First, the salient parts of the TLM prognostic equation for $\theta''$, using a two time level scheme and in coded form, are identified:

$$\theta''^{n+1}_{i,k} = \theta''^{n}_{i,k} + \frac{\Delta t}{2}\left[\tilde{\beta}^n_{k+1} w''^{n}_{i,k}\gamma^*_{k+1} + \tilde{\beta}^n_k w''^{n}_{i,k}\gamma^*_k\right] - \Delta t \tau_c^{-1}\theta''^{n}_{i,k} \tag{15}$$

The TLM variables are next replaced with their adjoint counterparts according to the EV procedure. This spawns the following three lines of adjoint code

$$\hat{w}^n_{i,k+1} \leftarrow \frac{\Delta t}{2}\tilde{\beta}^n_{i,k+1}\hat{\theta}^{n+1}_{i,k}\gamma^*_{k+1} \tag{16}$$

$$\hat{w}^n_{i,k} \leftarrow \frac{\Delta t}{2}\tilde{\beta}^n_{i,k}\hat{\theta}^{n+1}_{i,k}\gamma^*_{k} \tag{17}$$

$$\hat{\theta}^n_{i,k} \leftarrow -\Delta t \tau_c^{-1}\hat{\theta}^{n+1}_{i,k}, \tag{18}$$

where $\beta$ retains its previous meaning. The leftward directed arrow indicates an assignment to an equation that may also contain other terms. In building the prognostic expression for $\hat{w}^n_k$, for example, the right hand side of (17) will be one of the terms included.

Since the adjoint model is being integrated backward in time, time level $n+1$ "precedes" time level $n$. Expression (16) shows that potential temperature sensitivity at grid point $i$, $k$ and time level $n+1$ ($\hat{\theta}^{n+1}_{i,k}$) can influence vertical velocity sensitivity at $i$, $k+1$ and time $n$ ($\hat{w}^n_{i,k+1}$), but only if the time $n$ vertical velocity there was positive in the control run. As in the forward model, these terms affect the adjoint fields only in their respective, designated subdomains.

Automatic adjoint code generators typically produce a string of "line-by-line" code resembling the above. We note in passing that adjoint code often appears amenable to what we will term "recombination", resulting in a more readable and interpretable code, at least when periodic or solution specified boundary conditions are employed. Expression (16) can be remapped to point $i$, $k$ and combined with (17), yielding a single expression added to the right hand side of the $\hat{w}$ tendency equation. Indeed, the recombined result, being

$$\hat{w}^n_{i,k} \leftarrow \frac{\Delta t}{2}\tilde{\beta}^n_{i,k}\gamma^*_k\left[\hat{\theta}^{n+1}_{i,k} + \hat{\theta}^{n+1}_{i,k-1}\right], \tag{19}$$

appears to make good physical sense. In the forward TLM (12), the time $n$ vertical velocity averaged to the scalar location directly affects the temperature perturbation there at time $n+1$. In

the backward propagating adjoint model, the vertical velocity sensitivity at time $n$ is determined by the time $n$+1 temperature sensitivities, averaged to the $w$ location. Both are constrained by the behavior of the control run at time $n$, through $\beta$.

### 2.6 Verification of the TLM and adjoint

The control/TLM combination may fail to accurately reproduce the alternative run not only owing to the TLM's inherent approximations but also due to design and coding errors. Considerable effort was made to make sure the TLM was free of the latter error sources. The verified TLM model was then used to vet the correctness of the adjoint model's coding.

In the course of TLM model validation, the strictly adiabatic discretized model was examined first. In this configuration, inherent TLM error arises solely due to the neglect of terms beyond first order in the Taylor expansions. This truncation, however, affects only the advection terms, and the missing terms themselves are no higher than second order. Indeed, they are nothing other than easily identified TLM perturbation products.

We tested the adiabatic TLM model code by installing and temporarily reenabling these missing terms. The output of this "augmented" model should track the discrepancies between the control and alternative simulations to within roundoff error. This was found to be the case, thereby validating the adiabatic TLM code itself. Naturally, the perturbation product terms have to be excluded from the TLM since they cannot be written in matrix form, and thus are not transposable for use in the adjoint model.

The PM model's diabatic terms are first order but note (9) is not differentiable at $w = 0$. Thus, there is error beyond simple roundoff wherever and whenever the control and alternative simulation vertical velocities have different signs (as might happen if the updraft boundary were slightly shifted between two nonlinear simulations, for example). A formulation for (12) that is exact (to within roundoff error) is

$$\begin{aligned} Q''^{+}_{i,k} &= \frac{\Delta t}{2}\left[\{\max(\tilde{w}^n_{i,k+1} + w''^n_{i,k+1}, 0) - \max(\tilde{w}^n_{i,k+1}, 0)\}\gamma^*_{k+1}\right. \\ &\quad \left. + \{\max(\tilde{w}^n_{i,k} + w''^n_{i,k}, 0) - \max(\tilde{w}^n_{i,k}, 0)\}\gamma^*_k\right] \end{aligned} \tag{20}$$

but this is also not transposable. However, this formulation was used temporarily as a checking and assessment tool.

The verified TLM model was then used to vet the correctness of the adjoint model's coding via the gradient test. For adjoint simulations in general, a control simulation must first be made and archived. For adjoint validation runs, TLM forecasts are made and archived as well, and those data are used to calculate $\Delta J$ every time step during the backward integration. Recall that $\Delta J$ is temporally invariant when a two time level scheme is employed. In our tests with periodic lateral boundaries, the Euler backward version of the model can preserve $\Delta J$ to sixteen digits when double precision is used for all reals. As shown by TC, owing to the leapfrog's three time level structure, $\Delta J$ equivalence can only be shown for the first and final time steps. This equivalency was demonstrated by the leapfrog version of our adjoint modeling system.

Control run archiving was performed every time step for the simulations shown herein. This requires a large amount of storage. Significant savings may be realized by archiving at less frequent intervals (e.g., EV; Langland et al., 1995). In our model, the slow variation of the simulations' important modes permits this to be done with very little impact on the computed sensitivities. This will be exploited in the future.

## 3 A control run simulation

A simulation was made using the FT2000's low CAPE (convective available potential energy), low stability sounding graphically depicted in Fig. 1. The figure also illustrates the path taken by a parcel rising undiluted from the boundary layer. This parcel's level of free convection is at $z_b = 1$ km, and its maximum buoyancy ($\Delta_m$= 3K) is realized at $z_m = 7$ km. Above this point, we presume the parcel has run out of vapor. Its equilibrium level would reside at $z_t = 9$ km; the CAPE for this hypothetical parcel is 400 J kg$^{-1}$.

The base state horizontal wind profile (not shown) consisted of 9.75 m s$^{-1}$ of wind speed change over the lowest 3 km, starting with calm conditions at the surface and with zero shear farther aloft. Since vertical shear vector points eastward, we will refer to the west and east sides of the storm

as the "upshear" and "downshear" directions, respectively. The cooling zone was 1.5 km deep and 45 km wide, with $\theta_c'$ = -4.5K and $\tau_c$ = 600 s. The model was translated eastward at 11.5 m s$^{-1}$, effectively rendering the cold pool stationary. The model was run for 9000 s, more than enough time for the storm to develop and attain a statistically steady structure (see Fovell and Ogura 1988), at least in the vicinity of the convection, without significant artifacts owing to the enforced periodicity.

Figures 2 and 3 present perturbation fields of potential temperature, horizontal velocity ($u'$) and pressure ($p'$) along with vertical velocity $w$; for convenience, we have dispensed with the tildes. Note the $u'$ field is independent of the reference frame. The principal storm updraft was well formed by 3000 sec and already leaning rearward (upshear) over the cold pool (Figs. 2a, 3a). The lower tropospheric flow accelerated upward within the updraft split into two principal branches, the front-to-rear (FTR) flow which continued rearward, and the forward anvil outflow which overturned and spread upstream of the storm. The rear inflow current was established beneath the FTR flow, residing largely in the lower troposphere above the spreading cold pool.

The environment responded to the initiation of convective heating by generating compensating subsidence which spread in both directions away from the main convecting region as gravity waves. We will henceforth focus on the eastbound wave which propagated through the storm's upstream environment. Figure 3 shows its leading edge was marked by low surface pressure, leaving horizontal airflow that has been accelerated towards (away) from the convection in the lower (upper) troposphere in its wake. Uninterrupted positive buoyancy concentrated in the middle troposphere spans that region. This is a combination of the gravity wave's *in situ* subsidence warming and convectively generated warming exported in the forward anvil outflow.

The eastbound wave's domain-relative propagation speed was $\approx$ 10 m s$^{-1}$, making for a 21.5 m s$^{-1}$ ground-relative motion. The dependence of the phase speed $c$ on $H$, the vertical dimension of the diabatic source, is seen in (e.g., Nicholls et al. 1991)

$$c = \bar{u} + \frac{NH}{\pi}, \tag{21}$$

where $\bar{u}$ is the mean wind (9.75 m s$^{-1}$ above the shear layer), $N$ is the Brunt-Vaisalla frequency (.004 in the base state middle troposphere) and $\pi$ has its usual meaning. The expected $c$ = 21.5 m

$s^{-1}$ results when $H$ is taken to be 9 km.

# 4 Examination of forward anvil outflow strength with the adjoint model

The adjoint model was used to examine the dynamical precursors of the westerly upper tropospheric forward anvil outflow as it existed at 6000 sec. Basing $J$ on the $u$ field within the subsidence wave's leading edge and at the location indicated in Fig. 2b, we made the initial $\hat{u}$ field a function that was smoothly tapered from a unit maximum to zero over a 3000 m wide by 800 m deep region. This effectively makes our $J$ a weighted average of the $u$ field within the specified area[2].

In this application, positive $\Delta J$ values would represent further intensification of the westerly forward anvil outflow in the aspect region. As revealed by (5), this can be realized by applying positively (negatively) signed alterations where and when the adjoint model predicts positive (negative) sensitivity. As would be expected, the individual sensitivities are dynamically consistent with one another and combine to present a coherent picture. Examining each field's sensitivity in isolation, however, helps reveal not only how that field contributes to the whole but also what the impact of alterations in that field alone might be expected to be.

## 4.1 Adiabatic adjoint run

Two 3500 sec long backwards runs were made with this $J$, excluding and including the adjoint's diabatic terms. Excluding the moisture parameterization terms renders the adjoint model strictly adiabatic – and undoubtedly less accurate. Therefore, caution in interpretation is indicated, especially as sensitivities reach into the unstable region and cooling zone. Still, this simulation illustrates the adjoint model's utility as a dynamical tracer in convectively driven flows. The importance of the diabatic terms is assessed in the next section.

Figures 4 and 5 present contoured adjoint sensitivity fields superimposed upon shaded control run fields at 4000 sec, 2000 sec into this backward integration. Superposing sensitivity and forward

[2]The initial sensitivity represents an unbalanced jolt and using a smoother initial condition reduces the magnitude of the resulting acoustic activity.

model fields greatly facilitates interpretation. Since the forward anvil outflow and subsidence wave were thermally driven it is not surprising that sensitivity not only became chiefly concentrated in the temperature adjoint variable $\hat{\theta}$ but also backtracked towards the actively convecting region as time rewound[3]. Positive sensitivity appears in the warmed air just behind the subsidence feature's leading edge while negative $\hat{\theta}$ is found immediately above. The former implies that one way to make the aspect region's westerly anvil outflow stronger at 6000 sec is to further intensify the warm anomaly located above $x \approx 280$ km at 4000 sec. The latter indicates that the subsequent outflow could also be enhanced by cooling the neutrally buoyant air located above the warm anomaly.

These operations are sensible, both separately and jointly. Intensifying the already warm air behind the subsidence wave's leading edge would make the horizontal buoyancy gradient across that boundary larger, increasing the local generation of positive horizontal vorticity. As qualitatively depicted on the figure, the circulatory tendency associated with this vorticity generation would tend to encourage ascent in the warm anomaly itself as well as westerly flow above and to the east of it. Cooling the air above the warm anomaly would have the complementary effect of encouraging subsidence within the anomaly and westerly flow below and to the east of its center. Both of these westerly enhancements at the present time and place would reasonably lead to subsequent enhanced westerly flow in the aspect region farther downstream.

Furthermore, note that the largest positive sensitivity resides about 1 km above the location of the warmest air in the control run at 4000 sec. The adjoint model is indicating that shifting the present warm and cold anomalies closer together vertically – displacing the cooled (warmed) locale downward (upward) – would also serve to enhance the subsequent westerly outflow. This should indeed result because the buoyancy-induced outflows in this case would be concentrated into a still narrower layer, and would thus be intensified.

In the horizontal velocity field (Fig. 4b), the principal center of positive sensitivity is seen to be located in the forward anvil outflow at the 8 km level above $x \approx 280$ km, where $u$ values in the control run are positive (westerly). The adjoint model indicates that an increase in the anvil leading edge westerlies at 4000 sec will result in stronger winds in the forecast aspect region farther

[3]Please note that the contour intervals employed for $\hat{u}$, $\hat{p}$ and $\hat{w}$ in Figs. 4 and 5 are considerably smaller than that used for $\hat{\theta}$. Therefore, perturbations of substantially larger magnitude would need to be applied to these fields to accomplish a significant $\Delta J$.

downstream 2000 sec later. Thusfar, the adjoint model is providing reasonable, easily interpretable results.

For vertical velocity (Fig. 5a), the adjoint model again suggests that strenghtening the subsidence wave at the present time would lead to stronger westerly outflow in the aspect region later. In the range $270 < x < 290$ km, there is positive (negative) sensitivity attached to areas presently experiencing upward (downward) motions. Comparison with Fig. 4a shows these sensitivities are in quadrature with the $\hat{\theta}$ field, and consistent with eastward gravity wave phase propagation. Note some sensitivity has already reached into the main convecting region. There are other features in the sensitivity field as well, but keep in mind the overall magnitudes of $\hat{w}$ are extremely small.

The principal signature in the $\hat{p}$ field (Fig. 5b) is negative sensitivity in the middle troposphere, above the present surface low center. Perhaps lowering the pressure in the indicated region would increase the horizontal pressure gradient force exerted on parcels located farther west. This would accelerate the westerly flow in the forward outflow behind the subsidence wave's leading edge at the time depicted. Another interpretation has the adjoint model suggesting that a deepening of the already present low pressure anomaly now would strengthen the anvil outflow later. As the storm's total depth is constrained by the stable stratosphere, this might encourage the westerly flow to be squeezed into a shallower layer and thereby cause its intensification.

Figures 6 and 7 present the control run and sensitivity fields at 3000 sec. Again, the largest sensitivities are in the temperature field (Fig. 6a), and are especially concentrated in the warming near the subsidence feature's present location. Also notable is the significant negative temperature sensitivity located farther aloft. The cooling that was present there in the control run resulted from parcels in the storm's main updraft (compare with Fig. 7a) overshooting their level of neutral buoyancy. Note that the forward anvil outflow issues from, and is strongest within, the area between these sensitivity centers (Fig. 6b). The adjoint model is again indicating that anything that would serve to make these marked temperature anomalies stronger and closer together now would result in enhanced westerly flow in the aspect region later.

In addition to the expected positive $\hat{u}$ sensitivity in the forward anvil, an area of substantial negative sensitivity has appeared in the lower troposphere (Fig. 7b), straddling the gust front located at $x \approx$

265 km. Across this zone, the storm-relative control run flow switches from weak westerly behind the gust front to easterly ahead of it. The adjoint model predicts the subsequent forward anvil outflow would be intensified if that easterly flow were further enhanced (i.e., $u'' < 0$). Weakening the westerlies behind the front are expected to help, for reasons that are less immediately clear. Perhaps the sensitivities are attempting to impart a downshear tilt on the main storm airflow; such an orientation would direct more mass into the forward anvil. The effect of including the diabatic terms on the sensitivity field at this time is discussed below.

The $\hat{w}$ sensitivity in the main storm updraft (Fig. 7a) seems to suggest alterations that would shorten but also expand that feature laterally eastward. Either might help shift the cooling resulting from overshooting towards the east. The negative sensitivity above $x = 270$ km may be attempting to widen the subsidence wave's downdraft (located above $x = 275$ km) westward. Taken together, these alterations would sharpen the horizontal $w$ gradients across the east edge of the main storm updraft, perhaps leading to a stronger overall circulation including enhancement of the forward anvil's westerly flow.

The pressure adjoint field (Fig. 7b) suggests a similar interpretation now as at 4000 sec. However, significant sensitivity has reached the convecting region by this time, rendering the adiabatic restriction questionable. The diabatic adjoint run is examined next.

### 4.2 Diabatic adjoint run

Figures 8 and 9 present the sensitivity fields obtained at 3000 sec when the adjoint's diabatic terms were enabled[4] . Inclusion of the cooling zone term in the backward model had but a very small effect on the results. As expected, the parameterized warming term, active within the region indicated on Fig. 8a, exerted a significant impact by this time.

Outside of the unstable region, the temperature sensitivities (Fig. 8a) qualitatively resembled those from the adiabatic simulation. The diabatic adjoint run, however, put the largest sensitivity on the east side of the main storm updraft, just inside the unstable region. This warming is colocated with positive $\hat{w}$ sensitivity (Fig. 9a), suggesting that enhancing the updraft there (resulting in

[4]Please note that some contour intervals have been increased, particularly for $\hat{w}$.

more diabatic heating) in the forward model would help increase $J$. This appears tantamount to widening the main storm updraft.

Taken together, the $\hat{u}$ and $\hat{w}$ sensitivities suggest inducing a clockwise circulation anchored around $z = 6$ km above $x = 271$ km. This circulation would indeed encourage westerly flow into the forward anvil. As noted above, the adjoint's diabatic heating term drives the ascending branch of the circulation. Beyond the unstable region's east edge, the $\hat{w}$ and $\hat{\theta}$ sensitivities are in quadrature, likely suggesting eastward gravity wave propagation. The point of largest negative pressure sensitivity resides near the center of this circulation.

Overall, the importance of the adjoint's diabatic terms when applied to convectively driven flows has become clear. Since the westerly outflow is associated with the subsidence wave, anything that acts to strengthen the latter encourages the former. As the wave itself was triggered by the convection, wave intensification proceeds from convective enhancement. The adjoint model's suggestion of a wider storm updraft perhaps stands in part for an increase in the vertical mass flux. As additional mass is transported upward, more may be directed into the forward anvil, leading to a strengthening of the upper tropospheric westerlies so long as the thickness of the outflow layer is not increased. Recall the sensitivities above and beyond the unstable region appear to be encouraging a narrowing of that layer.

# 5 Examination of the lower tropospheric storm inflow with the adjoint model

## 5.1 Background

Storms exert a substantial impact on their surroundings, including the upstream environment into which they are propagating. This adjoint investigation was initiated to help explain differences between PM and traditional cloud model storms with regard to the magnitude and character of their upstream influence. Figure 10, adapted from FT2000, shows mature phase profiles of ground-relative horizontal wind taken 20 km ahead of the surface gust front position for three simulations which shared the same initial wind profile (also shown) and roughly comparable soundings. The

explicit moisture benchmark run (grey dashed line) was created with the ARPS[5] cloud model (Xue et al. 2000) using Fovell and Ogura's (1988; hereafter "FO") moderate CAPE sounding. The other two were PM simulations initialized with FT2000's modified FO environment. The PM simulations gauge the effect of a "convective sponge", FT2000's crude attempt to restrain the upstream influence (see below); the "basic model" run did not include this extra term. The difference between initial and disturbed profiles is $u'$.

All three model storms developed forward anvil outflows ($u' > 0$) in the upper troposphere, and mass continuity dictates there must be compensating inflow enhancement somewhere. The enhancement in the ARPS case was confined to a relatively shallow midtropospheric layer around 5 km, leaving the lower troposphere largely unmodified. In the basic PM model simulation, however, the inflow acceleration extended to the surface, with the maximum increase located very close to the ground. This is a significant difference. The cloud model storm's augmented inflow consisted of dry air which might be expected to weaken the convective intensity. In contrast, much of the basic PM storm's enhancement was potentially warm. The vertical shear in contact with the deep convective updraft differed markedly in the middle troposphere as well. While the low-level shear has the larger influence on the storm (Rotunno et al. 1988), the middle tropospheric shear is not itself unimportant (Garner and Thorpe 1992; Fovell and Dailey 1995).

FT2000 focused on the anvil outflow, regarding its significant – and apparently excessive – strength in the basic PM case as reflecting a fundamental deficiency in the parameterization. Positive midtropospheric temperature perturbations develop in a mature storm's trailing region, being a combination of *in situ* subsidence and latent heat release along with warming advected rearward by the FTR flow. In reality, latent heating wanes in the convective cells propagating through this region because they are being progressively starved of moisture. The moisture parameterization, however, permits such heating to continue as long as the updraft persists, and of course this heating serves to maintain the updraft. In this manner, the PM storms' trailing region temperature perturbations can become relatively substantial in magnitude. This can be seen for the present PM control run in Fig. 2.

The midtropospheric warming establishes high perturbation pressure in the upper troposphere

[5]The University of Oklahoma's Advanced Regional Prediction System.

poised above the warmed layer (e.g., Fig. 3). The PM model's exaggerated rear-side warming increased the temperature, and thus the pressure, contrast with the forward anvil region. FT2000 hypothesized that if the upper tropospheric horizontal pressure gradient force were reduced, both the anvil outflow and compensating lower tropospheric inflow would be weakened. To accomplish this, they fashioned a "convective sponge" to slowly remove positive temperature perturbations in the trailing region. As suggested by Fig. 10, the sponge could and did reduce the magnitude of both $u'$ features in the upstream environment. However, this artificial sponge did not resolve concerns regarding the inflow's vertical distribution or the midtropospheric shear. Indeed, decreasing the circulation's strength made it more readily apparent that the most important discrepancy lay in the *position*, rather than the magnitude, of the maximum enhanced inflow.

### 5.2 Sensitivity analysis using the adjoint model

What does it take to concentrate the enhanced inflow into the middle troposphere, at least in the vicinity of the convection? To address this, two separate diabatic adjoint simulations were started at time 9000 sec with horizontal velocity forecast aspects positioned in the upstream lower and middle troposphere, respectively (see Fig. 2c). The experiments were designed so that a positive $\Delta J$ – the result of pairing like-signed alterations and sensitivities – would represent a reduction in the low-level inflow and/or an intensification of the midlevel inflow. The lower tropospheric aspect was proportional to $u$ itself so $\Delta J > 0$ means weakening the pre-existing easterly wind perturbations. $J$ was defined as proportional to $-u$ in the middle tropospheric aspect so a positive $\Delta J$ increased those easterlies. Since the adjoint model is linear, the $J$ sign reversal is purely cosmetic.

Though the two adjoint runs were independent, they told the same story[6]. Again, the temperature variable quickly came to dominate the results, with both simulations concentrating negative sensitivity in the middle troposphere just upstream of the main storm updraft by 5500 sec (Fig. 11). The shaded field reveals the control run had some positive $\theta'$ in the sensitive region. A positive $\Delta J$ requires reducing that warming, or even instituting local *cooling*, at that location and time. Note the same negative temperature alterations that would decrease the low-level inflow would increase it at midlevels, thereby accomplishing a shift of the enhanced inflow from near the surface to 5 km,

[6]Implementing both aspects simultaneously yielded very similar results.

where the explicit moisture cloud model says it belongs.

These adjoint results motivated Fovell (2002) to revisit the upstream influence issue. There is indeed weak yet persistent local cooling present just ahead of the convective region in a typical traditional cloud model simulation (see Fig. 12), something that is absent from its PM counterpart (Fig. 2). (Note that Fig. 12's shading scheme deliberately emphasizes these small negative perturbations relative to their positive counterparts.) Fovell (2002) showed the weak upstream cooling represents the combined effect of cloud water evaporation and the forced ascent of subsaturated, midtropospheric air encountering the storm updraft. Although undoubtedly exaggerated somewhat in the 2D geometry, the latter effect is also quite pronounced in three-dimensional simulations as well (not shown).

The midtropospheric cooling is small in magnitude and quite localized, making it easy to miss amid the larger and more extensive temperature perturbations of both signs within, above and below the main updraft. Yet, this subtle perturbation turns out to have had a rather dramatic effect on the storm inflow structure. Fovell (2002) described the environmental upstream modification as a gravity wave response to not only the heating but also the cooling occurring in and around the main storm updraft. The initial heating provokes deep, rapidly propagating subsidence of the kind seen in Sec. 3; this established the enhanced low-level inflow. The persistent cooling that subsequently appears during maturity, however, excites a secondary gravity wave response, one characterized by lower tropospheric ascent. This wave also propagates (albeit more slowly) ahead of the storm, gently lifting the air approaching the main updraft. As a result, the inflow enhancement is shifted to the middle troposphere, cooling (and, in the explicit moisture model, moistening) the air in the process.

Thanks to FT2000's truncating the unstable region, the PM model is quite capable of handling any gravity wave response in the upstream environment; what was missing is the *cooling*. Naturally, the model has no cloud water to evaporate. However, the original PM framework's more serious flaw is that all ascending air in the unstable region is presumed to be saturated and thus generating condensation warming. In actuality, the air at an updraft's periphery may represent stable air that is and remains subsaturated upon ascent, as seen in Fig. 12. Fovell (2002) improved the moisture parameterization by allowing slowly ascending air to remain subsaturated. This made the PM

model results far more comparable to those from traditional cloud models (see his Figs. 13 and 14).

### 5.3 Discussion

FT2000's original hypothesis was based on excessive trailing region warming. It is telling that neither adjoint simulation placed sensitivity in the model storm's trailing region, at least by 5500 sec (Figs. 11a and 11b). To see whether any sensitivity would appear there at a still earlier time, the integrations were extended back to 3500 sec. That nothing significant rearward of the main updraft ever appeared is evidenced by the temperature sensitivity field for the middle tropospheric aspect (Fig. 11c). This explains why FT2000's convective sponge failed to resolve the discrepancies between the PM and explicit moisture model results. As reasonable as their hypothesis may have seemed, it didn't describe how the phenomenon in question actually came about in the model. Many paths to a particular outcome or result are possible, but we are by far most interested in discovering which path the *model* took. The usefulness of the adjoint model as a backwards dynamical tracer is hereby demonstrated.

The success of the improved moisture parameterization encouraged us to consider a more sophisticated adjoint formulation, one that has explicit moisture but the bare minimum of complexity. Figure 13 presents results from a "no-cloud cloud model" (NCCM), which combines the PM cooling zone with a typical cloud model saturation adjustment scheme. However, cloud water is removed as it is generated, so only the adjoint of the saturation adjustment itself is necessary. Cloud water evaporation is missing from the model, but analysis suggests its contribution is not necessary. Starting with the FO sounding, the NCCM model storm easily generates weak but persistent cooling upstream of the convective region and the elevated upstream inflow it provokes. Figure 13b presents the temperature sensitivity field at 5500 sec, resulting from the lower tropospheric $J$ consisting of horizontal velocity positioned as shown in Fig. 13a. The results confirm those obtained from the PM model and demonstrate that much of what makes traditional cloud models (and their adjoints) so very complicated can sometimes be neglected.

# 6 Summary

The adjoint of a parameterized moisture (PM) convection model was described and tested. Adjoint models are useful for tracing features back to their dynamical origins, facilitating hypothesis construction and testing. However, such models can be difficult to construct and are based on sometimes worrisome linearity assumptions. Certainly, cloud microphysics, including the saturation process, are very complicated, involving numerous nonlinearities and interactions as well as binary switches. The PM framework dramatically reduces the model's complexity by specifying the location and magnitude of evaporation cooling and by making latent heating conditionally proportional to vertical velocity. Its adjoint is simple and linear, and can be implemented with little error.

However, the PM adjoint's usefulness is limited if the moisture parameterization cannot produce reasonable results. Naturally, there are many things a PM model can never simulate. However, our previously cited reservations (Fovell and Tan 2000) concerned the degree of influence exerted by PM model storms on the environments into which they are propagating. Compared to explicit moisture cloud models, PM convection generated overly strong forward anvil outflows and put the compensating tropospheric inflow far too close to the surface. The strength and nature of the enhanced upstream inflow is very different for PM and explicit moisture storms, at least in the immediate vicinity of the convection.

Fovell and Tan (2000) advanced a hypothesis to explain the discrepancies between the models but the "fix" that hypothesis motivated did not appreciably improve the results. The PM model adjoint results described herein pointed to an entirely different, and previously overlooked, cause. Motivated by these results, Fovell (2002) revisited the upstream influence issue. Thus, in this application, the adjoint proved to be instrumental in disproving one hypothesis and suggesting another, leading to an improvement of both the PM model framework and our understanding of convective storms. The PM results also motivated a more sophisticated, but still relatively simple, adjoint that explicitly includes vapor but ignores water following condensation. Further applications of the PM and the "no-cloud cloud model" adjoints will be explored in the future.

*Acknowledgments*. This work was supported by NSF grant ATM-0139284.

# Appendix

Issues faced when using the three time level leapfrog (LF) scheme in an adjoint modeling system are demonstrated using a simple advection equation for TLM variable $u''$. This discussion represents an amplification of Talagrand and Courtier's (1987) Appendix C. When alterations to a constant advection speed $C_x$ are ignored, the TLM equation is

$$\frac{\partial u''}{\partial t} = -C_x \frac{\partial u''}{\partial x}. \tag{22}$$

Discretization using leapfrog time and center space differencing yields

$$u''^{n+1}_i = u''^{n-1}_i - \frac{C_x 2\Delta t}{2\Delta x}\left[u''^{n}_{i+1} - u''^{n}_{i-1}\right]. \tag{23}$$

The initial condition (IC) for the forward model is placed in $u''^{0}_i$ for any or all $i$. Integration commences with a forward (Euler) time step, coded as

$$u''^{1}_i = u''^{0}_i - \frac{C_x \Delta t}{2\Delta x}\left[u''^{0}_{i+1} - u''^{0}_{i-1}\right]. \tag{24}$$

For time steps $n = 1$, $N$-1, the standard LF is coded as:

$$u''^{n+1}_i = u''^{n-1}_i - \frac{C_x 2\Delta t}{2\Delta x}\left[u''^{n}_{i+1} - u''^{n}_{i-1}\right]. \tag{25}$$

Time step $N$-1 concludes with the final forecast representing time $N$.

Thus, for all time steps except the first, the LF scheme fuses information from time levels $n-1$ and $n$ into the forecast for time $n+1$ (Fig. A-1, upper panel). The adjoint of (24), proceeding in reverse, unravels this by placing information from time $n+1$ into both the $n$ and $n-1$ time levels. In other words, the $n+1$ time level was influenced by two prior times in the forward model, so in the reverse model it influences two earlier times (Fig. A-1, lower panel). This is seen in the following adjoint code, used for time steps $n$=$N$-1...1:

$$\hat{u}^{n-1}_i \leftarrow \hat{u}^{n+1}_i \tag{26}$$

$$\hat{u}^{n}_{i+1} \leftarrow -C_x \frac{2\Delta t}{2\Delta x}\hat{u}^{n+1}_i \tag{27}$$

$$\hat{u}^{n}_{i-1} \leftarrow +C_x \frac{2\Delta t}{2\Delta x}\hat{u}^{n+1}_i. \tag{28}$$

The backward integration concludes with the adjoint of (24), which is:

$$\hat{u}_i^0 \leftarrow \hat{u}_i^1 \tag{29}$$

$$\hat{u}_{i+1}^0 \leftarrow -C_x \frac{\Delta t}{2\Delta x} \hat{u}_i^1 \tag{30}$$

$$\hat{u}_{i-1}^0 \leftarrow +C_x \frac{\Delta t}{2\Delta x} \hat{u}_i^1. \tag{31}$$

All information is finally combined into the single, final time level.

The chief disadvantage of LF time differencing is that adjacent times must be combined to obtain a complete adjoint sensitivity field for at any intermediate time step between the first and final times. This is illustrated in Fig. A-2 for the present example. Consider an adjoint IC consisting of a single grid point (i.e., $\hat{u}_i^N$), indicated by the white dot labeled "0". Stepping from time step $N$ to $N$-1 with (26)-(28), this IC leads to information being placed into three time/space locales: $\hat{u}_{i+1}^{N-1}$, $\hat{u}_{i-1}^{N-1}$ and $\hat{u}_i^{N-2}$. The points involved in this first adjoint operation bear the label "1" in Fig. A-2. The next time step affects the locales marked "2". The time/space locale $(i, N-2)$ is being modified for the second time, so it bears both labels. At the conclusion of the third adjoint time step, the IC's influence has spread to the locales designated "3".

Though the example ceases at this point, the staggering has become obvious. It is clear that in order to retrieve a full intermediate field, two adjacent time levels would have to be combined. Further, this temporal-spatial separation isn't finally cured or "congealed" until the very last LF operation, the Euler step. It is that operation that finally stitches the odd and even time level fields together. This represents a significant limitation that is not shared by models employing two time level schemes.

## References


Arakawa A, Lamb V (1977): Computational design of the basic dynamical processes of the UCLA general circulation model. Methods Comput Phys 17: 174-267.

Cacuci DG, Hall MCG (1984): Efficient estimation of feedback effects with application to climate models. J Atmos Sci 41: 2063-2068.

Chorin AJ (1967): A numerical method for solving incompressible viscous flow problems. J Comput Phys 2: 12-16.

Errico RM (1997) What is an adjoint model? Bull Amer Meteor Soc 78: 2577-2591.

Errico RM, Vukicevic T (1992) Sensitivity analysis using an adjoint of the PSU-NCAR mesoscale model. Mon Wea Rev 120: 1644-1660.

Fovell RG (2002) Upstream influence of numerically simulated squall-line storms. Quart J Roy Meteor Soc 128: 893-912.

Fovell RG, Dailey PS (1995): The temporal behavior of numerically simulated multicell-type storms, Part I: Modes of behavior. J Atmos Sci 52: 2073-2095.

Fovell RG, Ogura Y (1988): Numerical simulation of a midlatitude squall line in two dimensions. J Atmos Sci 45: 3846-3879.

Fovell RG, Tan P-H (2000) A simplified squall-line model revisited. Quart J Roy Meteor Soc 126: 173-188.

Garner, ST, Thorpe AJ (1992): The development of organized convection in a simplified squall-line model. Quart J Roy Meteor Soc 118: 101-124.

Ghil M, Ide K, Bennett AF, Courtier P, Kimoto M, Sato N, editors (1997) Data Assimilation in Meteorology and Oceanography: Theory and Practice. Tokyo: Meteorological Society of Japan and Universal Academy Press, 496 pp.

Haltiner GJ, Williams RT (1980): Numerical Weather Prediction and Dynamic Meteorology. New York: Wiley, 477 pp.

Klemp JB, Wilhelmson RB (1978): The simulation of three-dimensional convective storm dynamics. J Atmos Sci 35: 1070-1096.

Langland RH, Elsberry RL, Errico RM (1995): Evaluation of physical processes in an idealized extratropical cyclone using adjoint sensitivity. Quart J Roy Meteor Soc 121: 1349–1386.

Langland RH, Gelaro R, Rohaly GD, Shapiro MA (1999): Targeted observations in FASTEX: Adjoint-based targeting procedures and data impact experiments in IOPs-17 and 18. Quart J Roy Meteor Soc 125: 3241-3270.

Lorenz EN, Emanuel KA (1998): Optimal sites for supplementary weather observations: Simulations with a small model. J Atmos Sci 55: 399-414.

Nicholls ME, Pielke RA, Cotton WR (1991): Thermally forced gravity waves in an atmosphere at rest. J Atmos Sci 48: 1869-1884.

Park SK, Droegemeier KK (1999): Sensitivity analysis of a moist 1-D Eulerian cloud model using automatic differentiation. Mon Wea Rev 127: 2128-2142.

Park SK, Droegemeier KK (2000): Sensitivity analysis of a 3D convective storm: Implications for variational data assiimilation and forecast error. Mon Wea Rev 128, 140-159.

Rabier F, Klinker E, Courtier P, Hollingsworth A (1996): Sensitivity of forecast errors to initial conditions. Quart J Roy Meteor Soc 122: 121-150.

Reed RJ, Kuo Y-H, Albright MD, Gao K, Guo Y-R, Huang W (2001): Analysis and modeling of a tropical-like cyclonein the Mediterranean Sea. Meteor Atmos Phys 76: 183-202.

Rosmond TE (1997): A technical description of the NRL adjoint modeling system. Naval Research Laboratory, Monterey, CA, publication NRL/MR/7532/97/7230.

Rotunno R., Klemp JB, Weisman ML (1988): A theory for strong, long lived squall lines. J Atmos Sci 45: 463-485.

Talagrand O, Courtier P (1987) Variational assimilation of meteorological observations with the adjoint vorticity equation. I: Theory. Quart J Roy Meteor Soc 113: 1311-1328.

Xu Q (1996): Generalized adjoint for physical processes with parameterized discontinuities. Part I: Basic issues and heuristic examples. J Atmos Sci 53: 1123-1142.

Xue M, Droegemeier KK, Wong V (2000): The Advanced Regional Prediction System (ARPS) – a multi-scale nonhydrostatic atmospheric simulation and prediction model. Part I: Model dynamics and verification. Meteor Atmos Phys 75: 161-193.

Zou X (1997): Tangent linear and adjoint of "on/off" processes and their feasibility for use in 4-dimensional variational data assimilation. Tellus 49A: 3-31.

**Figure captions**

Figure 1 - Schematic model illustrating PM model design. Fovell and Tan's (2000) low CAPE sounding is depicted at right. See text.

Figure 2 - Perturbation fields of potential temperature $\theta'$ (shaded; K) and horizontal velocity $u'$ (3 m s$^{-1}$ contours) for the control run. The zero contour is suppressed. Only a portion of the domain is shown.

Figure 3 - As in Fig. 2, but for perturbation pressure $p'$ (shaded; hPa) and vertical velocity $w$ (3 m s$^{-1}$ contours). Additionally, the -1 m s$^{-1}$ vertical velocity contour has been included.

Figure 4 - Control (shaded) and adjoint sensitivity (contoured) fields at 4000 sec: (a) perturbation potential temperature field $\hat{\theta}$ (.05 m s$^{-1}$ K$^{-1}$ contours); (b) horizontal velocity field $\hat{u}$ (.0075 [nondimensional] contours). Control field is full, storm-relative $u$ rather than $u'$. Shown in panel (a) is the circulatory tendency implied by the adjoint sensitivity field.

Figure 5 - As in Fig. 4, but showing: (a) vertical velocity sensitivity field $\hat{w}$ (.001 [nondimensional] contours); (b) perturbation pressure sensitivity field $\hat{p}$ (.002 m s$^{-1}$ hPa$^{-1}$ contours).

Figure 6 - As in Fig. 4, but at 3000 sec. Temperature sensitivity contour interval is .025 m s$^{-1}$ K$^{-1}$; for the horizontal velocity sensitivity it is .005 (nondimensional).

Figure 7 - As in Fig. 5, but at 3000 sec. Vertical velocity sensitivity contoured at .002 (nondimensional) intervals; for the pressure sensitivity it is .001 m s$^{-1}$ hPa$^{-1}$.

Figure 8 - As in Fig. 6, but for the diabatic adjoint run. Temperature sensitivity contour interval is .03 m s$^{-1}$ K$^{-1}$; for the horizontal velocity sensitivity it is .005 (nondimensional).

Figure 9 - As in Fig. 7, but for the diabatic adjoint run. Vertical velocity sensitivity contour interval is .003 (nondimensional); for the pressure sensitivity it is .0015 m s$^{-1}$ mb$^{-1}$).

Figure 10 - Instantaneous mature phase vertical profiles of ground-relative horizontal wind, taken at a location 20 km upstream of the surface gust front position for an ARPS model simulation

and PM model runs made without and with a "convective sponge" term. Also shown is the initial, undisturbed wind profile. The FO-MOD sounding was derived from Fovell and Ogura's (1988; "FO") initial environment, used in the ARPS run. Note that the PM runs did not employ the sounding in Fig. 1. After Fovell and Tan (2000).

Figure 11: Control (shaded) and adjoint sensitivity (contoured) fields of perturbation potential temperature for: (a) the lower tropospheric aspect at 5500 sec; (b) the middle tropospheric aspect at 5500 sec; and (c) the middle tropospheric aspect at 3500 sec. See Fig. 2c for locations of these aspects.

Figure 12 Perturbation fields of potential temperature (shaded; K) and horizontal velocity (3 m $s^{-1}$ contours) for a typical explicit moisture simulation, made using ARPS and the FO sounding. Updraft outline is $w = 1.75$ m $s^{-1}$. Color table chosen emphasizes the small cooling residing at and upstream of the leading edge.

Figure 13 Control (shaded) and adjoint sensitivity (contoured) fields from a no-cloud cloud model (NCCM) simulation made with the FO sounding, showing: (a) perturbation horizontal velocity with initial forecast location superposed; and (b) perturbation potential temperature and sensitivity (0.1 K s $m^{-1}$ contours).

Figure A-1: Schematic illustrating the leapfrog scheme in the forward TLM and adjoint models.

Figure A-2: Schematic illustrating why odd and even time steps in the adjoint integration do not separately yield full solutions for steps between the initial and final times when the leapfrog scheme is employed.

Mailing address:

Prof. Robert G. Fovell
Department of Atmospheric Sciences
University of California, Los Angeles
405 Hilgard Ave
Los Angeles, CA 90095-1565

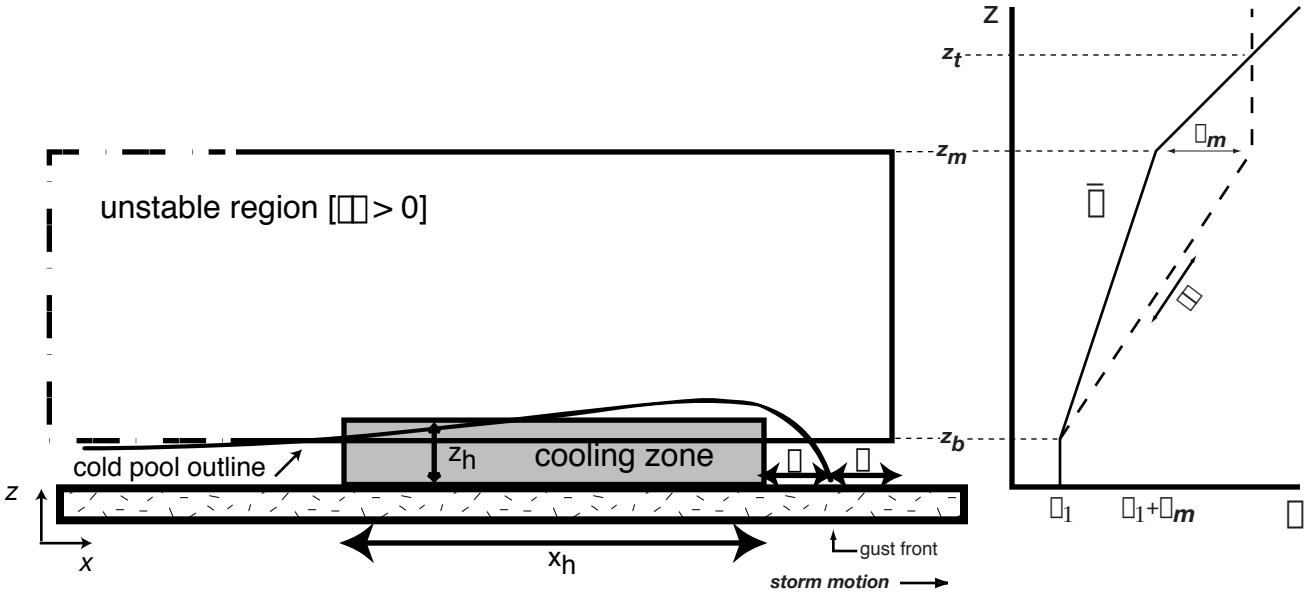
z
$z_t$
$z_m$
$z_b$
unstable region [□□ > 0]
cold pool outline
$z_h$
cooling zone
□
□
z
x
$x_h$
gust front
storm motion
□m
□
□
□1
□1+□m
□

***Figure 1***

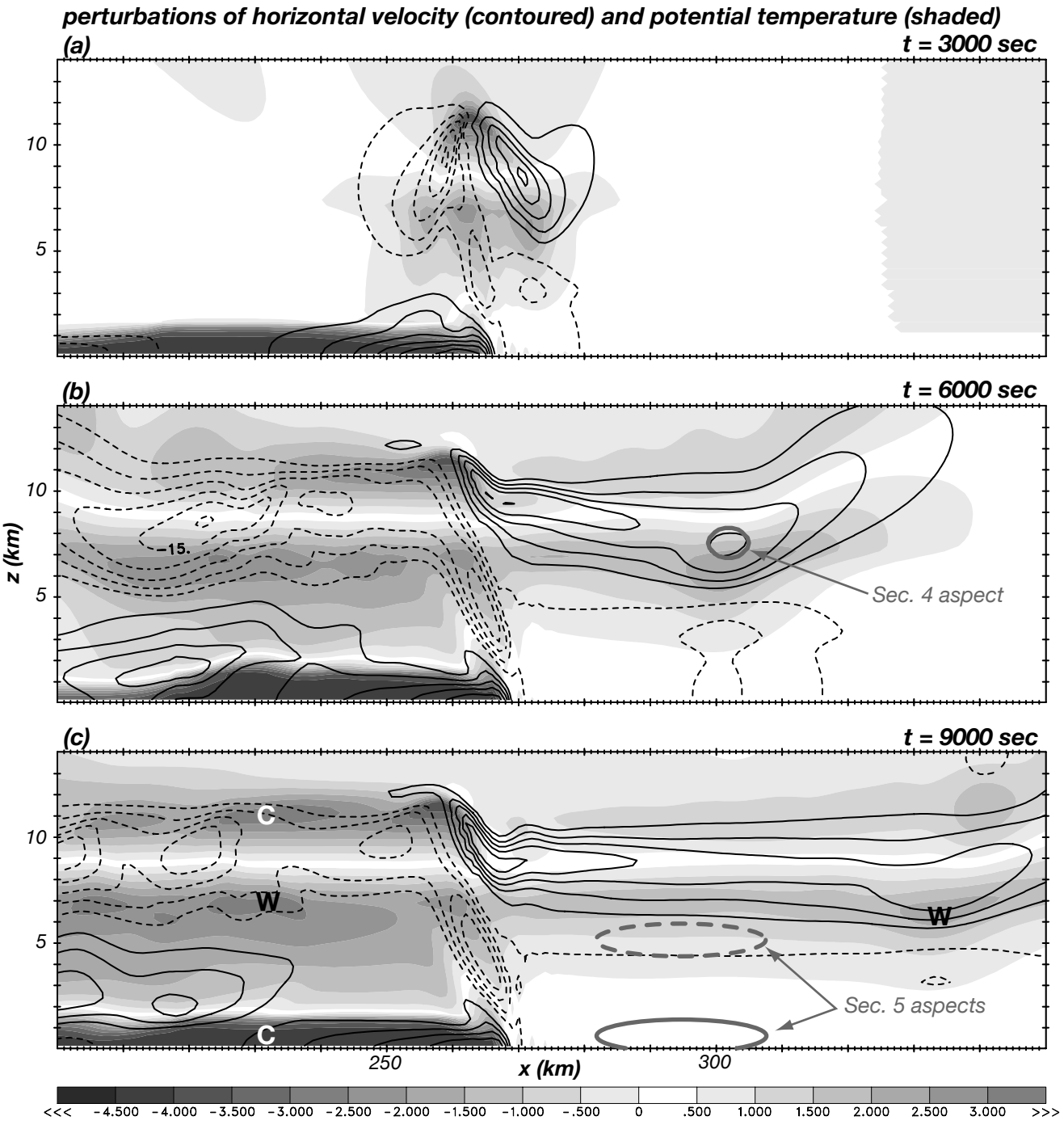
perturbations of horizontal velocity (contoured) and potential temperature (shaded)
(a)
t = 3000 sec
(b)
t = 6000 sec
(c)
t = 9000 sec
10
5
z (km)
-15.
Sec. 4 aspect
C
W
W
C
Sec. 5 aspects
250
x (km)
300
<<< -4.500 -4.000 -3.500 -3.000 -2.500 -2.000 -1.500 -1.000 -.500 0 .500 1.000 1.500 2.000 2.500 3.000 >>>

***Figure 2***

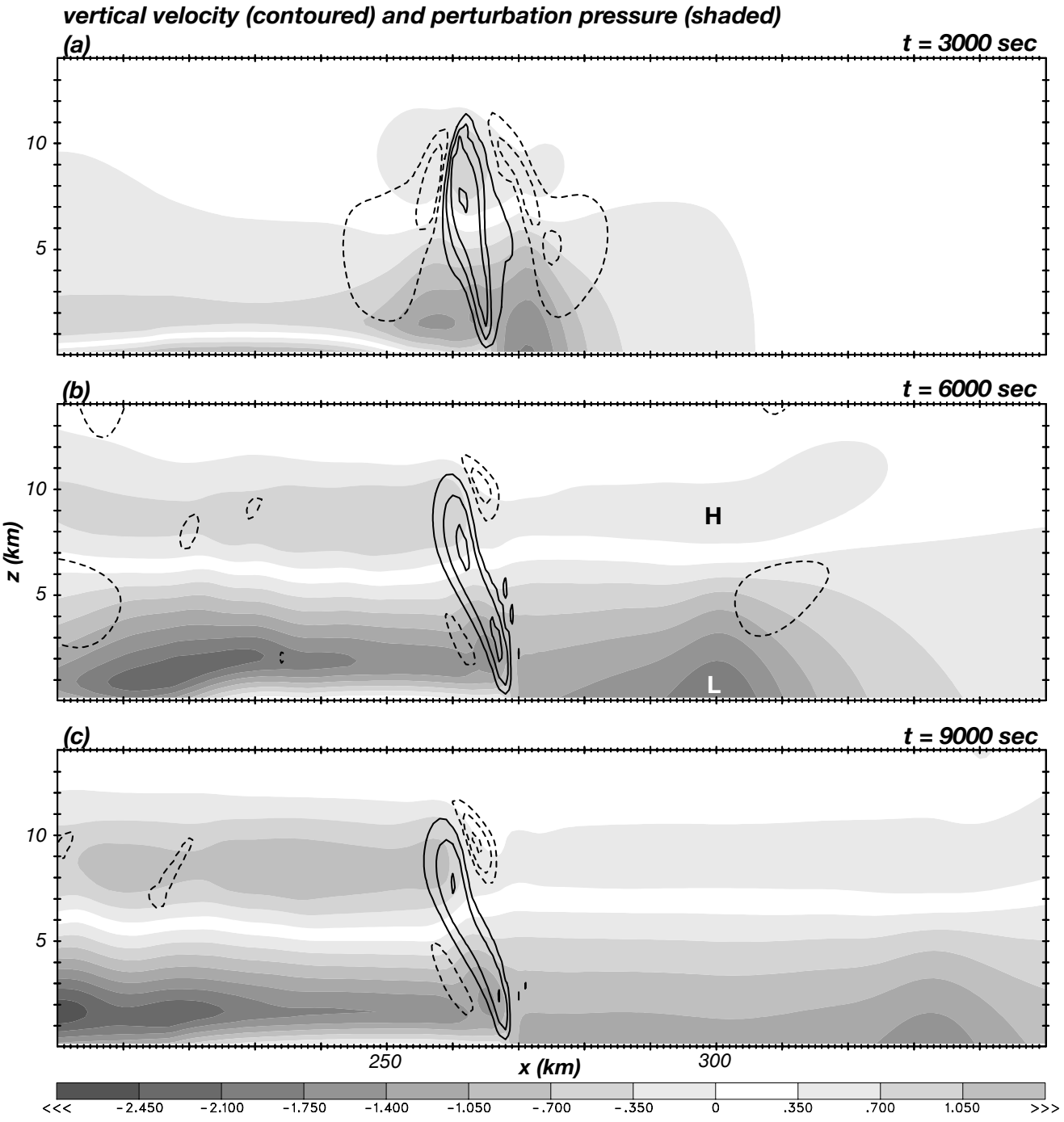
vertical velocity (contoured) and perturbation pressure (shaded)
(a)
t = 3000 sec
10
5
(b)
t = 6000 sec
H
L
z (km)
10
5
(c)
t = 9000 sec
10
5
250
x (km)
300
<<<
-2.450
-2.100
-1.750
-1.400
-1.050
-.700
-.350
0
.350
.700
1.050
>>>

***Figure 3***

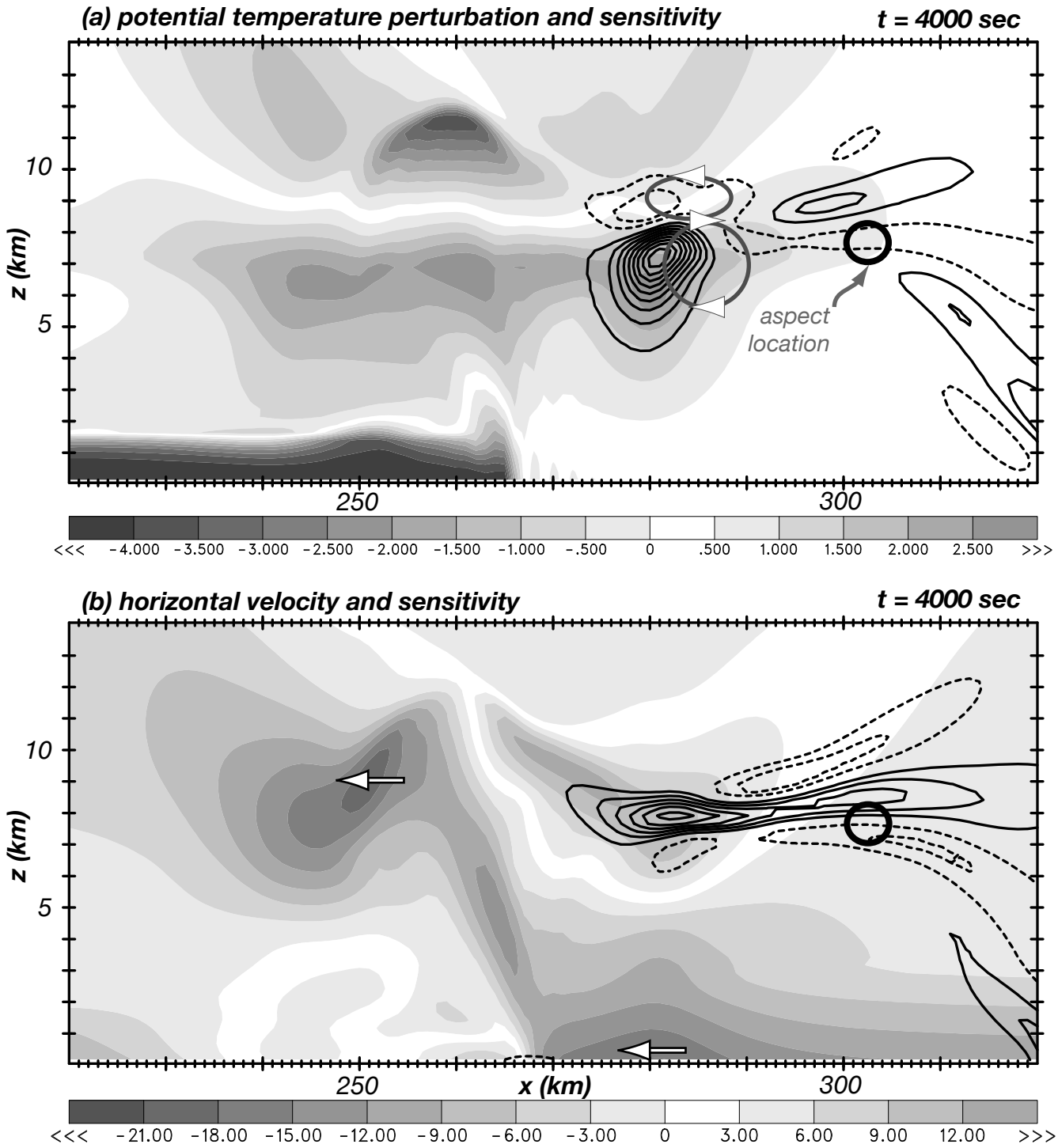
(a) potential temperature perturbation and sensitivity
t = 4000 sec
10
5
z (km)
aspect
location
250
300
<<< -4.000 -3.500 -3.000 -2.500 -2.000 -1.500 -1.000 -.500 0 .500 1.000 1.500 2.000 2.500 >>>
(b) horizontal velocity and sensitivity
t = 4000 sec
10
5
z (km)
250
x (km)
300
<<< -21.00 -18.00 -15.00 -12.00 -9.00 -6.00 -3.00 0 3.00 6.00 9.00 12.00 >>>

***Figure 4***

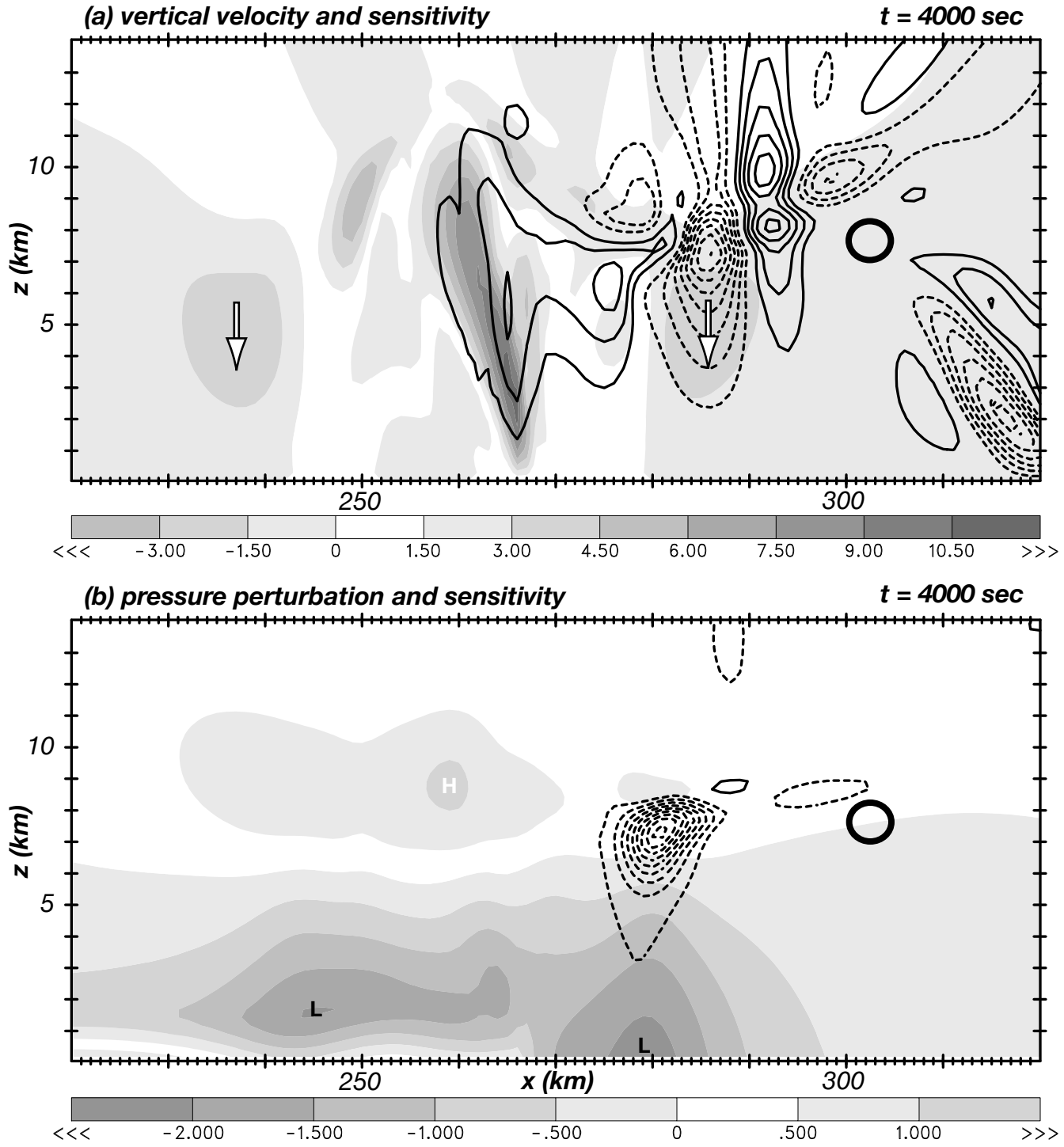
(a) vertical velocity and sensitivity
t = 4000 sec
z (km)
10
5
250
300
<<< -3.00 -1.50 0 1.50 3.00 4.50 6.00 7.50 9.00 10.50 >>>
(b) pressure perturbation and sensitivity
t = 4000 sec
z (km)
10
5
H
L
L
250
x (km)
300
<<< -2.000 -1.500 -1.000 -.500 0 .500 1.000 >>>

***Figure 5***

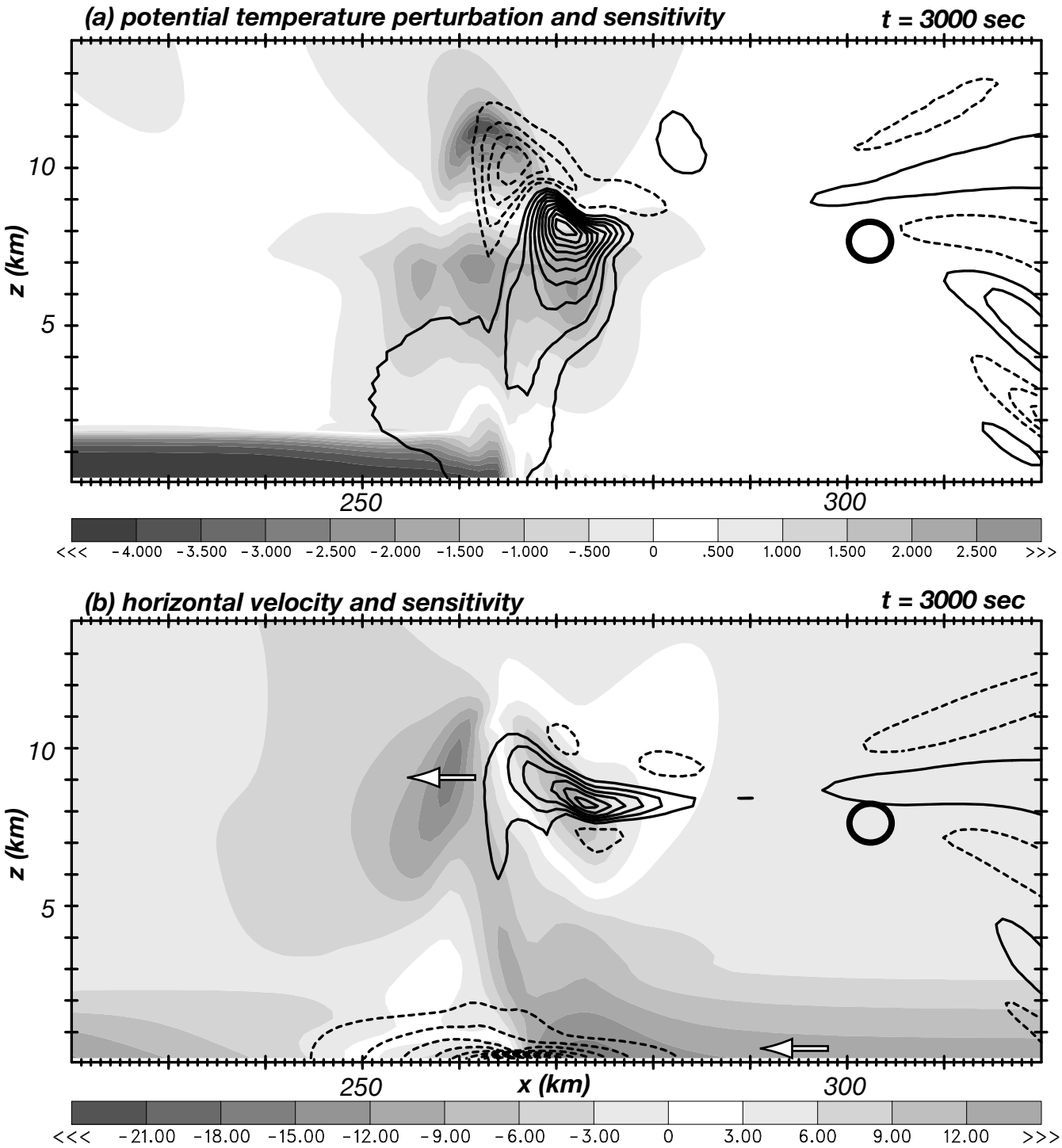
(a) potential temperature perturbation and sensitivity
t = 3000 sec
z (km)
10
5
250
300
<<< -4.000 -3.500 -3.000 -2.500 -2.000 -1.500 -1.000 -.500 0 .500 1.000 1.500 2.000 2.500 >>>
(b) horizontal velocity and sensitivity
t = 3000 sec
z (km)
10
5
250
x (km)
300
<<< -21.00 -18.00 -15.00 -12.00 -9.00 -6.00 -3.00 0 3.00 6.00 9.00 12.00 >>>

***Figure 6***

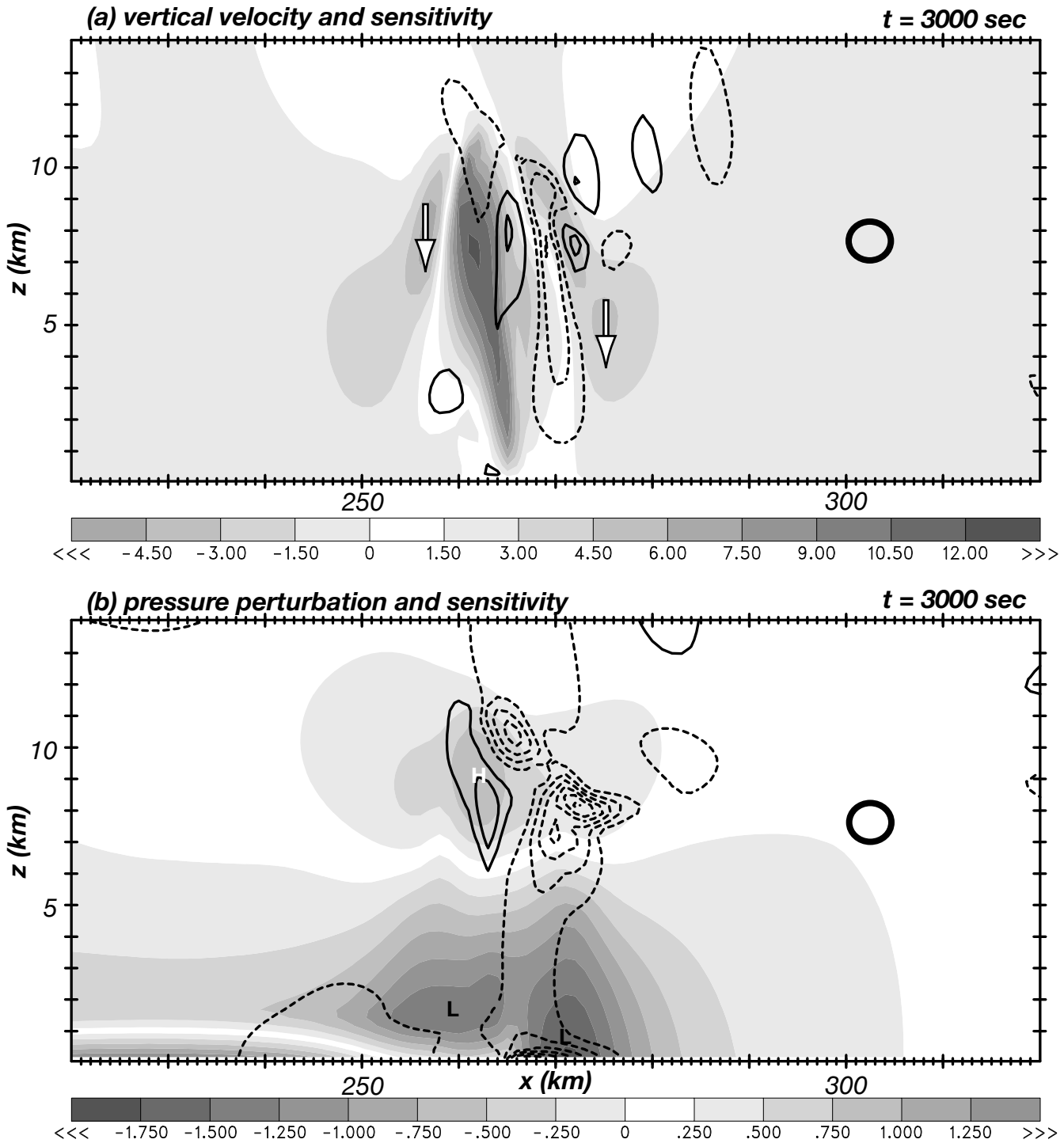
(a) vertical velocity and sensitivity
t = 3000 sec
z (km)
10
5
250
300
<<< -4.50 -3.00 -1.50 0 1.50 3.00 4.50 6.00 7.50 9.00 10.50 12.00 >>>
(b) pressure perturbation and sensitivity
t = 3000 sec
z (km)
10
5
H
L
L
250
x (km)
300
<<< -1.750 -1.500 -1.250 -1.000 -.750 -.500 -.250 0 .250 .500 .750 1.000 1.250 >>>

*Figure 7*

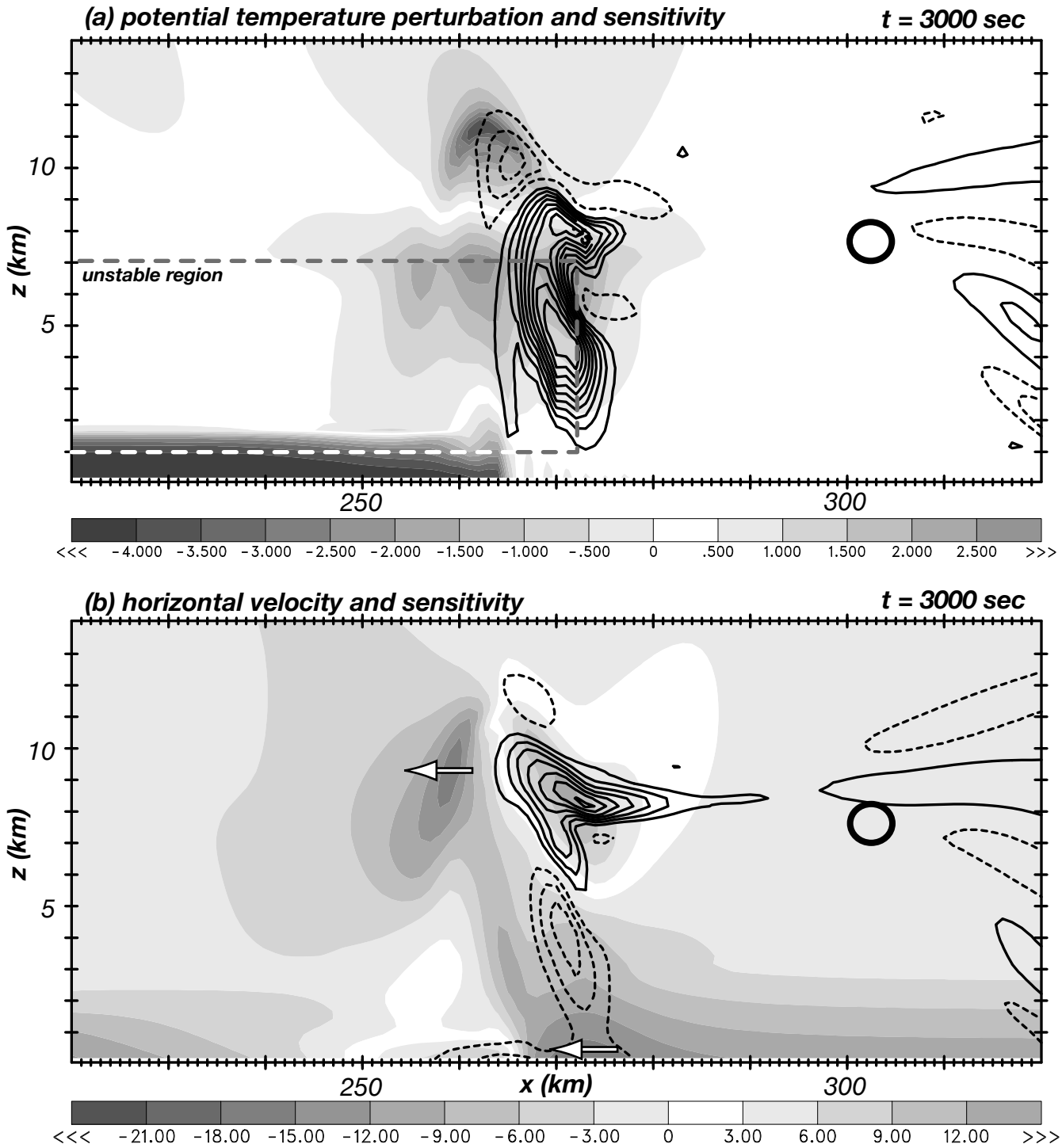
(a) potential temperature perturbation and sensitivity
t = 3000 sec
10
z (km)
5
unstable region
250
300
<<< -4.000 -3.500 -3.000 -2.500 -2.000 -1.500 -1.000 -.500 0 .500 1.000 1.500 2.000 2.500 >>>
(b) horizontal velocity and sensitivity
t = 3000 sec
10
z (km)
5
250
x (km)
300
<<< -21.00 -18.00 -15.00 -12.00 -9.00 -6.00 -3.00 0 3.00 6.00 9.00 12.00 >>>

***Figure 8***

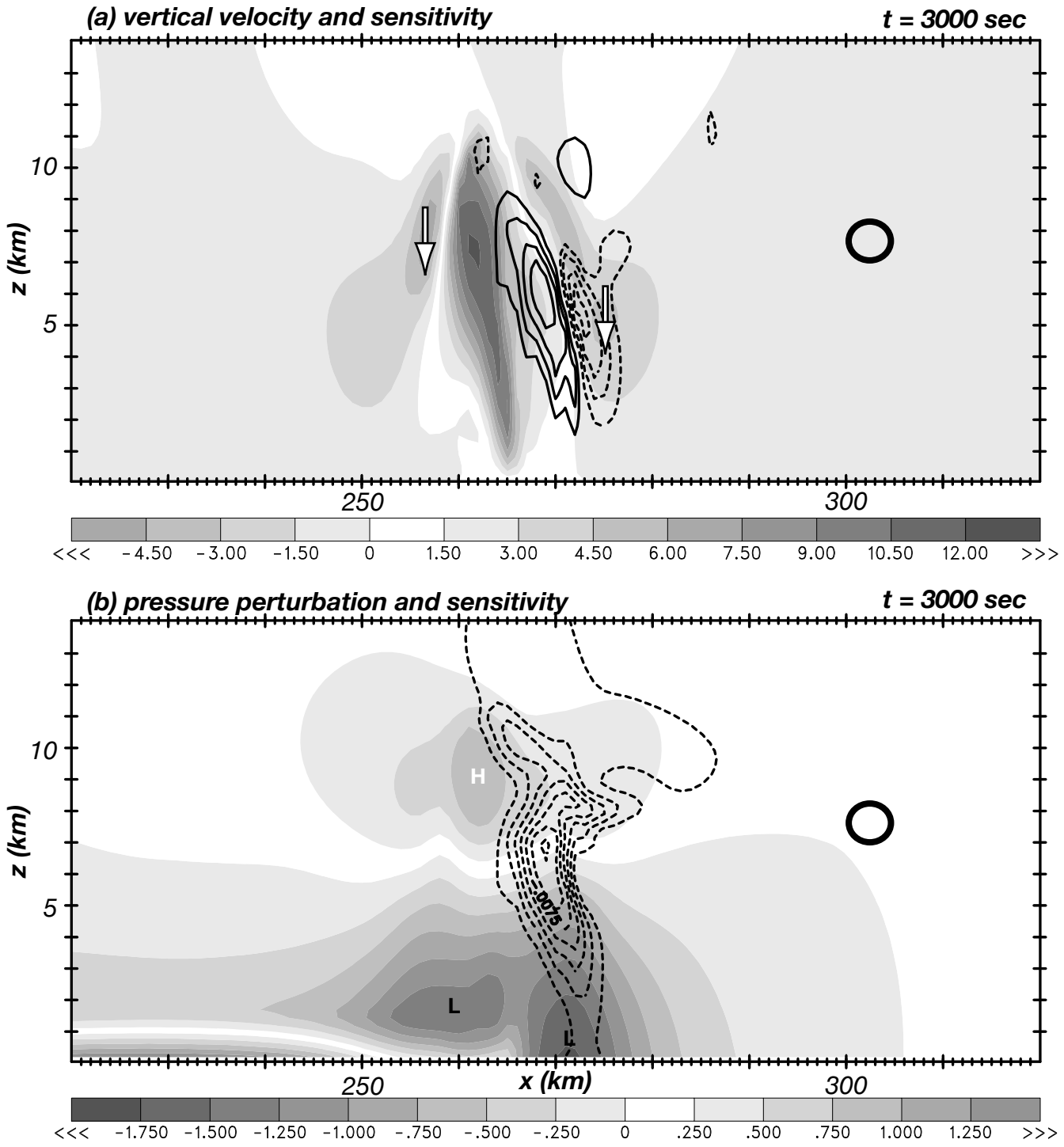
(a) vertical velocity and sensitivity
t = 3000 sec
z (km)
10
5
250
300
<<< -4.50 -3.00 -1.50 0 1.50 3.00 4.50 6.00 7.50 9.00 10.50 12.00 >>>
(b) pressure perturbation and sensitivity
t = 3000 sec
z (km)
10
5
H
L
L
.0075
250
x (km)
300
<<< -1.750 -1.500 -1.250 -1.000 -.750 -.500 -.250 0 .250 .500 .750 1.000 1.250 >>>

***Figure 9***

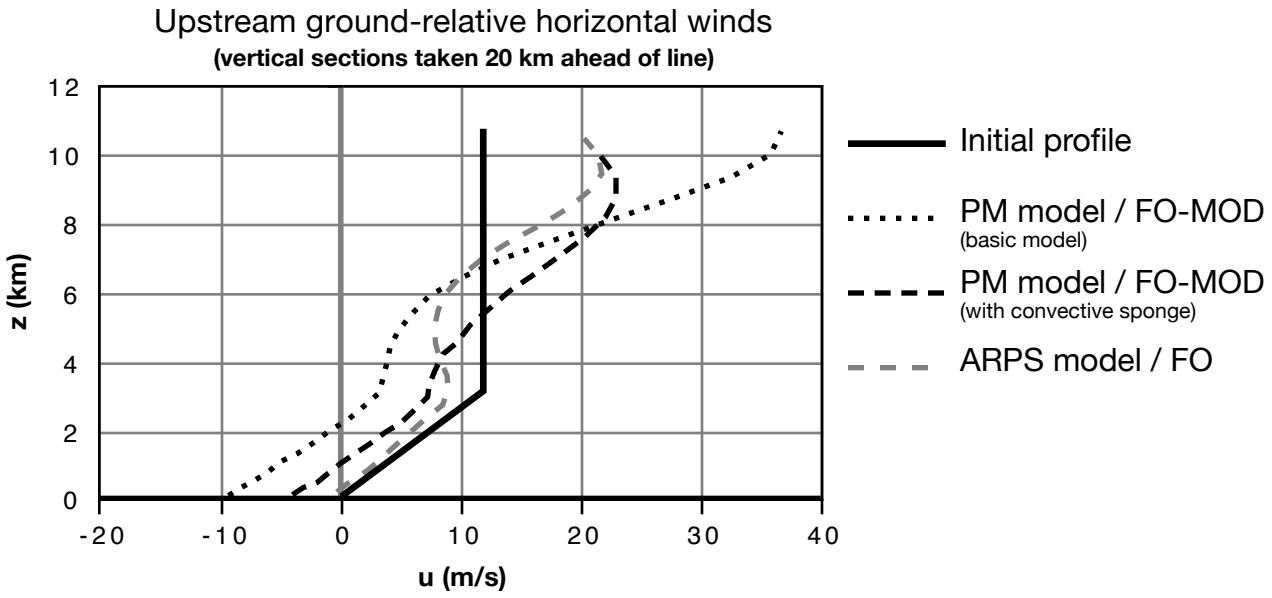
Upstream ground-relative horizontal winds
(vertical sections taken 20 km ahead of line)
z (km)
12
10
8
6
4
2
0
-20
-10
0
10
20
30
40
u (m/s)
Initial profile
PM model / FO-MOD
(basic model)
PM model / FO-MOD
(with convective sponge)
ARPS model / FO

***Figure 10***

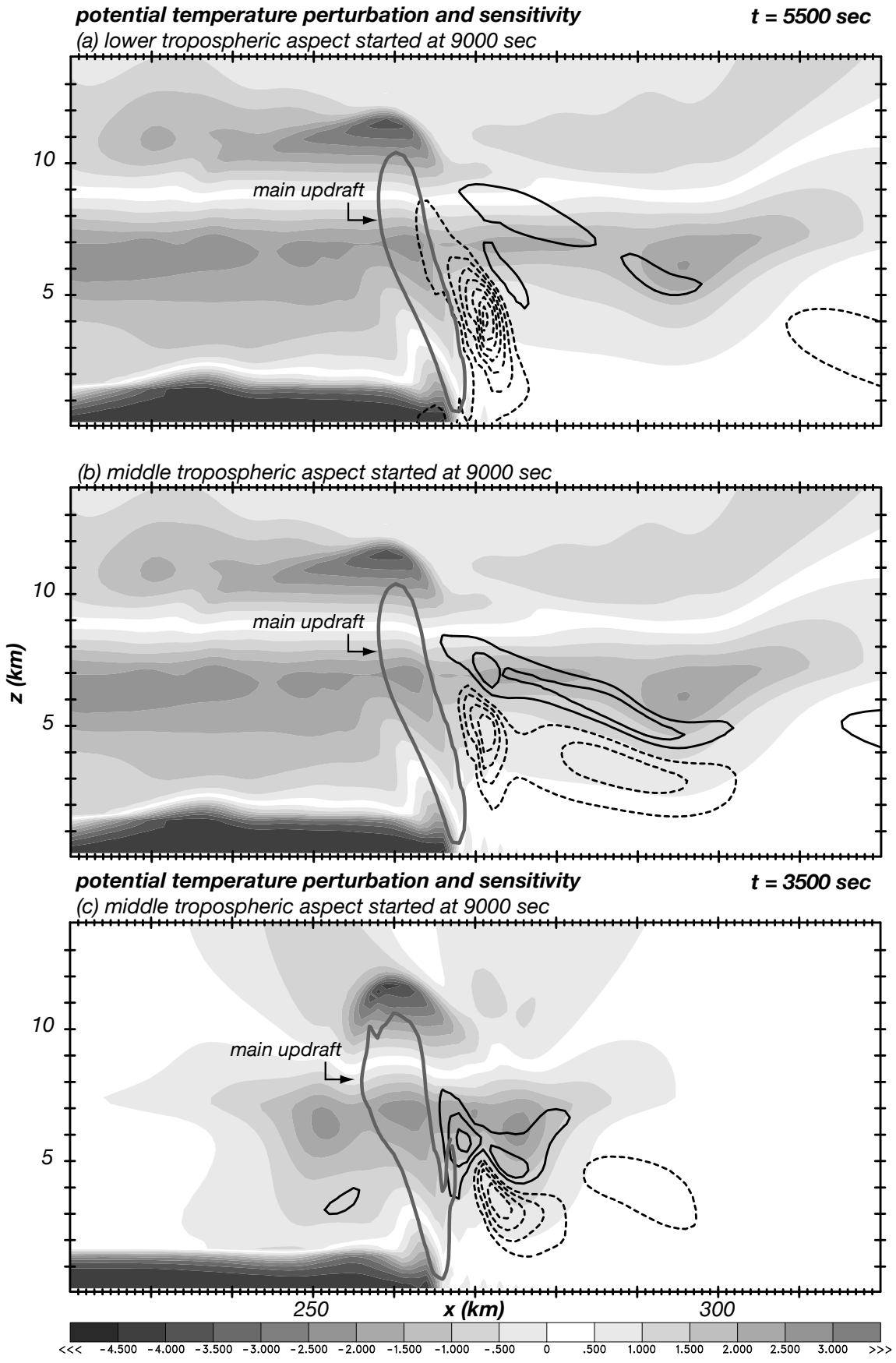
potential temperature perturbation and sensitivity
t = 5500 sec
(a) lower tropospheric aspect started at 9000 sec
main updraft
10
5
(b) middle tropospheric aspect started at 9000 sec
main updraft
z (km)
potential temperature perturbation and sensitivity
t = 3500 sec
(c) middle tropospheric aspect started at 9000 sec
main updraft
250
x (km)
300
<<< -4.500 -4.000 -3.500 -3.000 -2.500 -2.000 -1.500 -1.000 -.500 0 .500 1.000 1.500 2.000 2.500 3.000 >>>

***Figure 11***

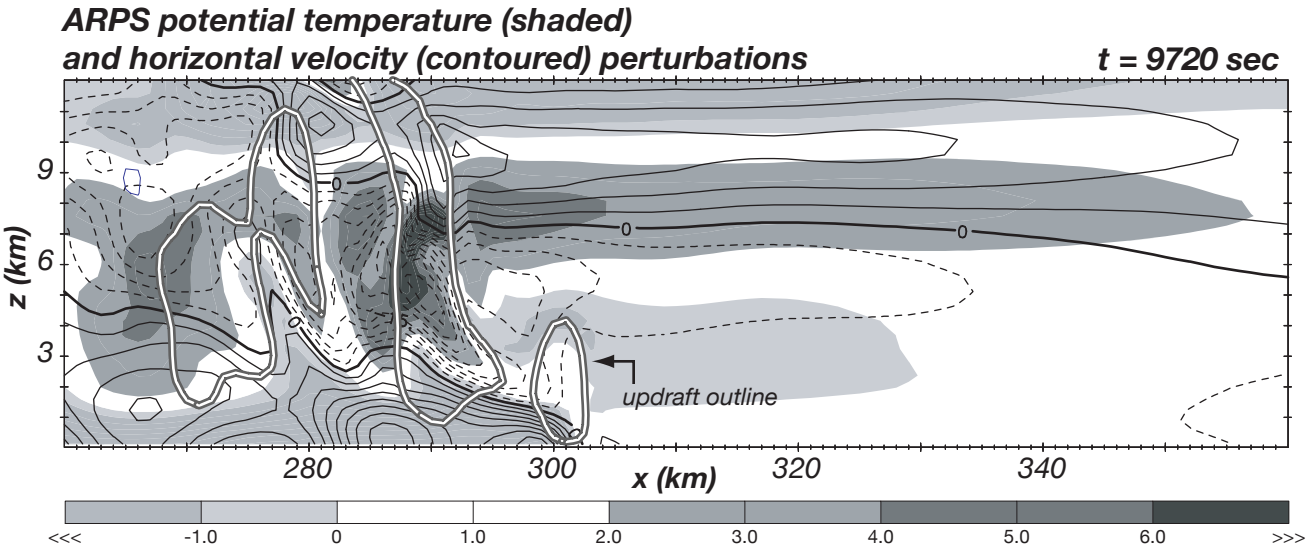
ARPS potential temperature (shaded)
and horizontal velocity (contoured) perturbations
t = 9720 sec
z (km)
9
6
3
0
0
0
0
updraft outline
280
300
320
340
x (km)
<<<
-1.0
0
1.0
2.0
3.0
4.0
5.0
6.0
>>>

***Figure 12***

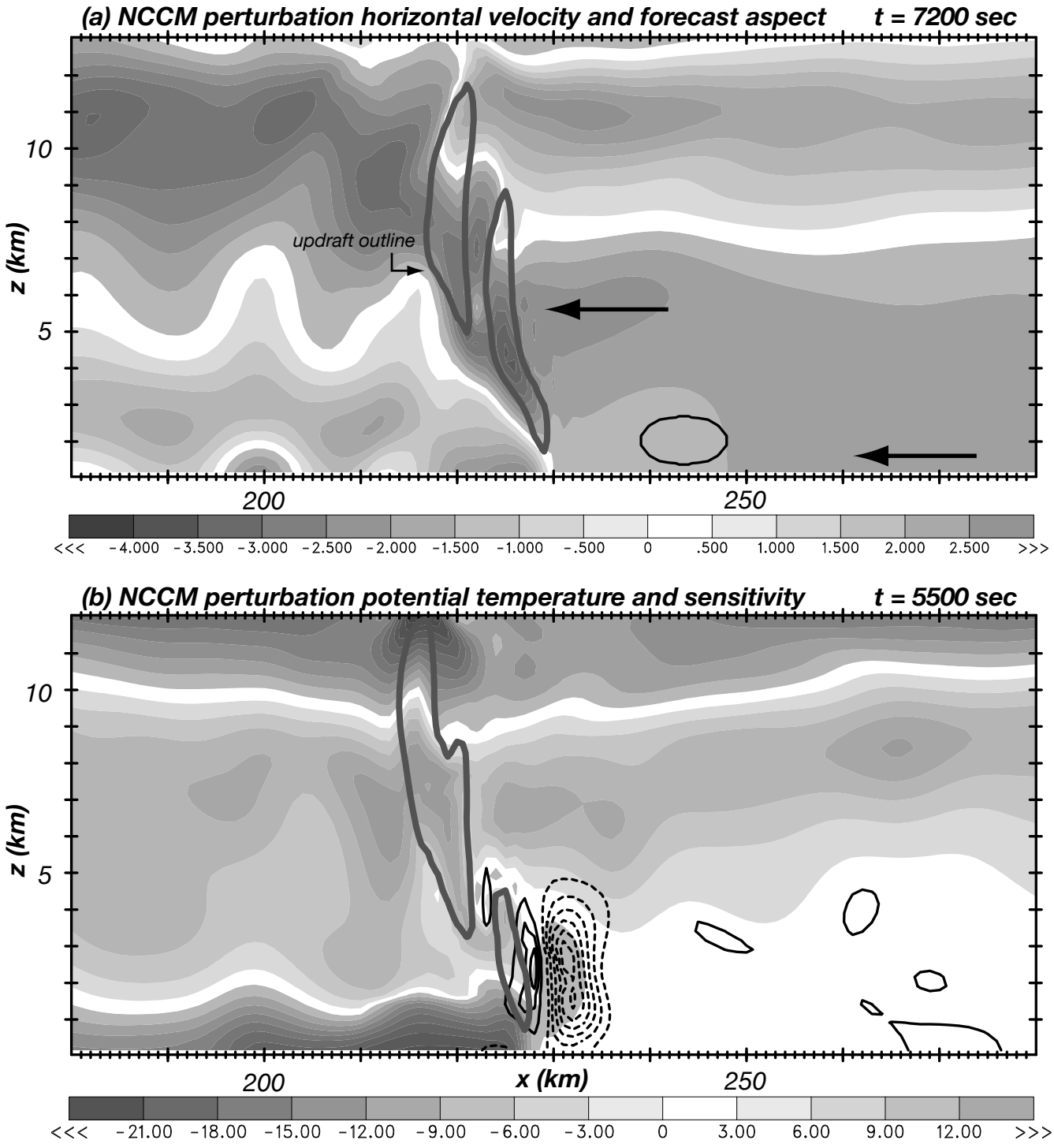
(a) NCCM perturbation horizontal velocity and forecast aspect t = 7200 sec
10
z (km)
5
updraft outline
200
250
<<< -4.000 -3.500 -3.000 -2.500 -2.000 -1.500 -1.000 -.500 0 .500 1.000 1.500 2.000 2.500 >>>
(b) NCCM perturbation potential temperature and sensitivity t = 5500 sec
10
z (km)
5
200
x (km)
250
<<< -21.00 -18.00 -15.00 -12.00 -9.00 -6.00 -3.00 0 3.00 6.00 9.00 12.00 >>>

***Figure 13***

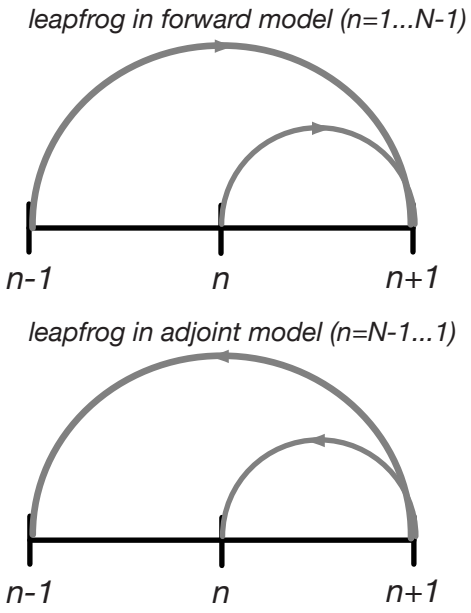
leapfrog in forward model (n=1...N-1)
n-1
n
n+1
leapfrog in adjoint model (n=N-1...1)
n-1
n
n+1

***Figure A-1***

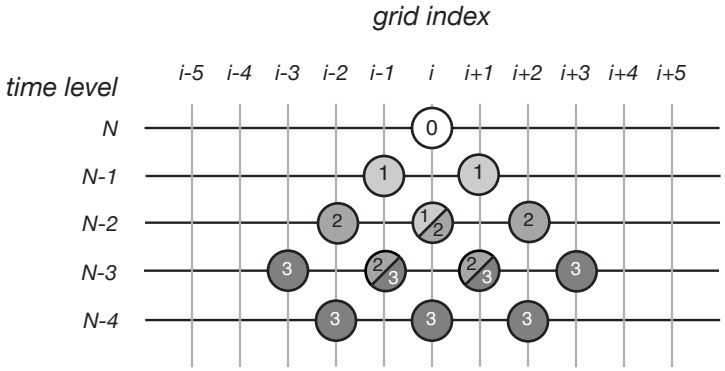
grid index
time level
i-5
i-4
i-3
i-2
i-1
i
i+1
i+2
i+3
i+4
i+5
N
N-1
N-2
N-3
N-4
0
1
1
2
1/2
2
3
2/3
2/3
3
3
3
3

***Figure A-2***